GEOLOGICAL JOURNAL
Geol. J. **41**: 23–48 (2006)
Published online 25 October 2005 in Wiley InterScience (www.interscience.wiley.com). DOI: 10.1002/gj.1031

Carbonate melting and peperite formation at the intrusive contact between large mafic dykes and clastic sediments of the upper Palaeozoic Saint-Jules Formation, New-Carlisle, Quebec

P. JUTRAS[1], A. MACRAE[1], J.V. OWEN[1], J. DOSTAL[1], M. PRÉDA[2] and G. PRICHONNET[2]*

[1]*Department of Geology, Saint Mary's University, Halifax, NS, B3H 3C3, Canada*
[2]*GEOTERAP, Département des Sciences de la Terre et de l'Atmosphère, Université du Québec à Montréal, C.P. 8888, Succ. Centre-Ville, Montréal, QC, H3C 3P8, Canada*

The base of an upper Palaeozoic graben-fill in eastern Canada was affected by mafic dyke intrusions shortly after deposition, resulting in the formation of peperite. Complex magma–sediment interactions occurred as the melts mingled with the wet and poorly consolidated clastic material of this sedimentary basin, which is separated from underlying rocks by the Acadian unconformity (Middle Devonian). As a result of these interactions, the mafic rocks are strongly oxidized, albitized and autobrecciated near and above the unconformity, where blocky juvenile clasts of mafic glass and porphyritic basalt have mingled with molten or fluidized sediments of the upper Palaeozoic Saint-Jules Formation, forming a peperite zone several metres thick. In contrast to most peperite occurrences, the New-Carlisle peperites are associated with the tip of dykes rather than with the sides of sills or dykes. We argue that more heat can be concentrated above a dyke than above a sill, as the former provides a more efficient and focused pathway for heated waters to invade the poorly consolidated host sediments. Superheated groundwaters that issued from the sides of the dykes appear to have promoted melting of carbonate components in calcareous sedimentary rock clasts of the Saint-Jules Formation, locally generating carbonate melts that contributed to the mingling of juvenile and sedimentary clasts in the peperite. Copyright © 2005 John Wiley & Sons, Ltd.

Received 1 December 2004; revised version received 26 May 2005; accepted 6 July 2005

KEY WORDS peperite; carbonate melting; upper Palaeozoic; mafic dykes; alteration; Canada

1. INTRODUCTION

The area of New-Carlisle, on the Quebec side of Chaleur Bay, Canada, is the host of large, closely spaced mafic dykes (Bagdley 1956; Jutras and Prichonnet 2004) (Figure 1). The dyke swarm is concentrated within an inlier of middle Palaeozoic rocks that is unconformably overlain by upper Palaeozoic rocks, but the dykes also intrude the base of the upper Palaeozoic succession (Figures 1, 2). During their emplacement, the mafic melts underwent major transformations as they reached the local Acadian (Middle Devonian) unconformity due to a sudden change in host material, from well-lithified fine-grained Silurian strata to coarse-grained and poorly consolidated Upper Devonian strata. Large exposures of the igneous bodies at the level of this unconformity allow detailed observations to be made concerning these transformations.

This paper describes the complex alteration profile that developed in the mafic rocks at New-Carlisle as the rising melts reached the local Acadian unconformity. It also presents evidence for the development of ferrocarbonatite and

* Correspondence to: P. Jutras, Department of Geology, Saint Mary's University, Halifax, NS, B3H 3C3, Canada.
E-mail: pierre.jutras@smu.ca
Contract/grant sponsor: Natural Sciences and Engineering Research Council of Canada.

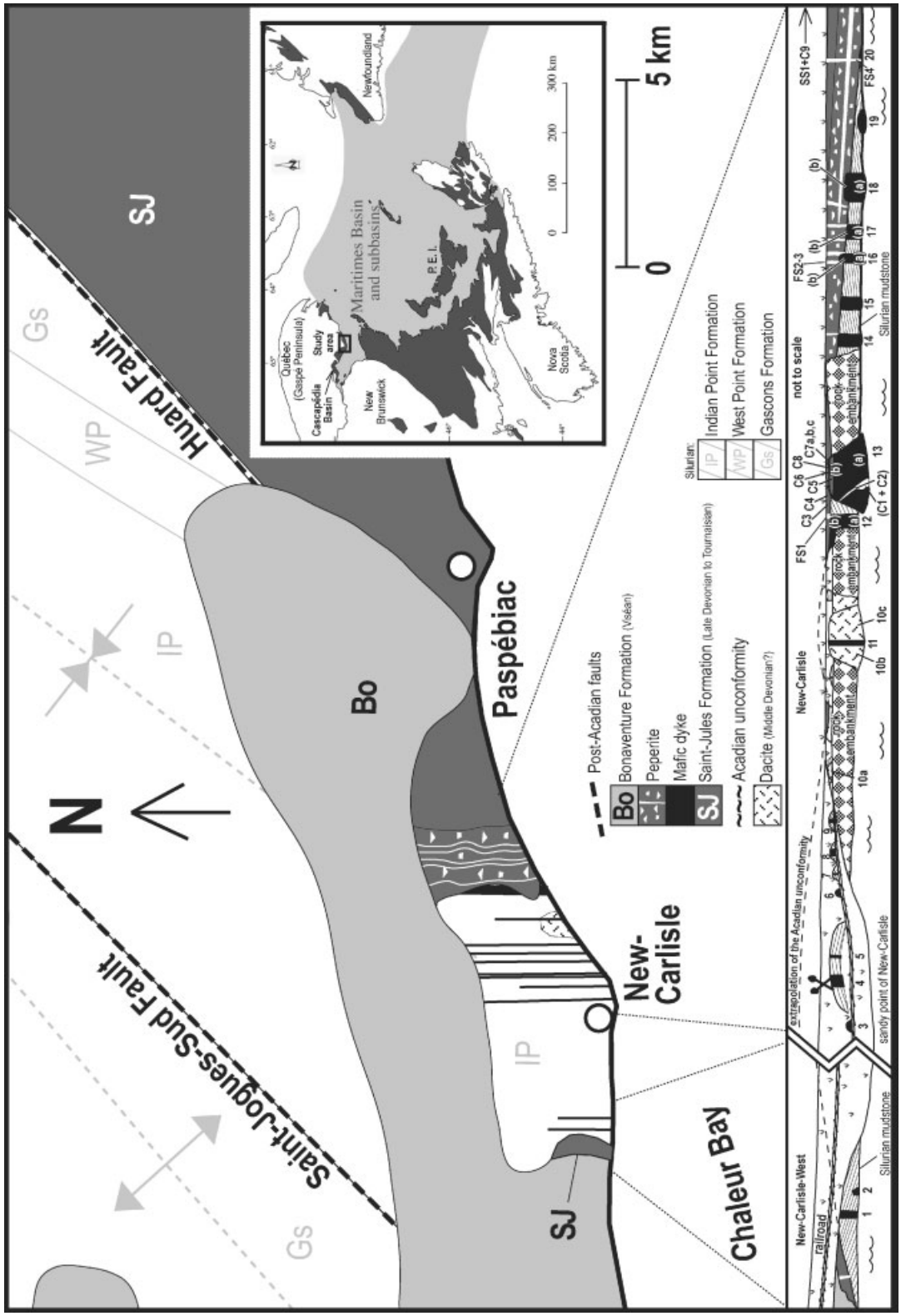

Figure 1. Geology of the New-Carlisle area, with a sketch of the dyke localities at the bottom (C = carbonate sample; FS = fluidized sand sample (sandstone dyke or sill); SS = sandstone sample). The pre-Devonian geology is by Bourque and Lachambre (1980). Inset: locality of the study area within the upper Palaeozoic Maritimes Basin (dark grey, inland; light grey, offshore).

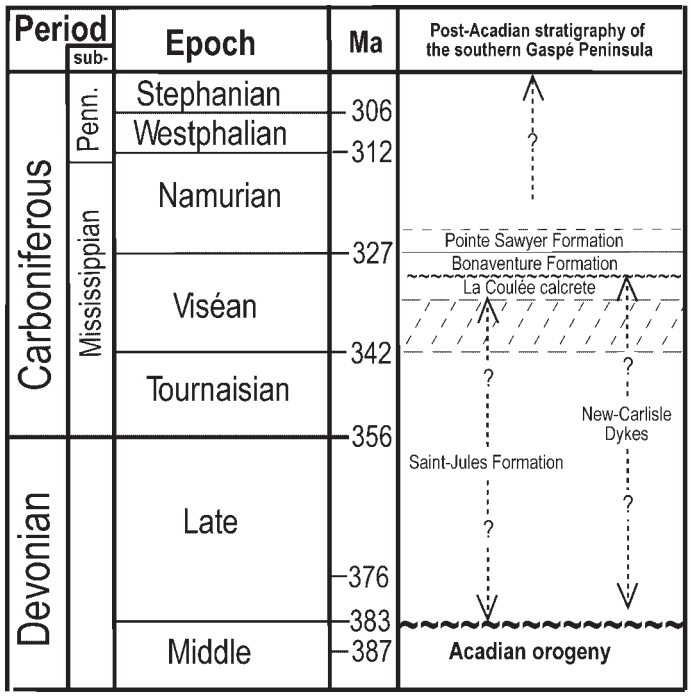

Figure 2. Post-Acadian stratigraphy of the southeastern Gaspé Peninsula. The time scale is after Okulitch (1999).

peperite from the interaction between magma and wet clastic sediments that were mainly composed of calcareous rock clasts. The study supports the conclusions of Lentz (1999) that carbonatites may not be exclusively derived from mantle melts. Finally, contrary to most documented peperites, which are located along the sides of sills (Brooks *et al.* 1982; Hanson and Schweickert 1982; Busby-Spera and White 1987; Branney and Suthren 1988; Krynauw *et al.* 1988; Boulter 1993; Brooks 1995; Coira and Pérez 2002; Dadd and van Wagoner 2002; Squire and McPhie 2002), the sides of dykes (Leat and Thompson 1988; Kano 1989; Goto and McPhie 1996; Hooten and Ort 2002; McClintock and White 2002) or above laccoliths (Coira and Pérez 2002), the New-Carlisle occurrences are located at the termination of dykes and were seemingly more thoroughly invaded by hydrothermal fluids than previously reported peperite occurrences.

2. REGIONAL GEOLOGY AND FIELD RELATIONS

Contacts between the mafic dykes and three types of host rock are well exposed in shoreline outcrops. The oldest of the host rocks are calcareous mudstones of the Upper Silurian Indian Point Formation (Bagdley 1956; Bourque and Lachambre 1980), which are intruded by a previously unreported porphyritic and nodular dacite plug (Figure 1, locality 10, and Figures 3, 4). The dacite is separated from the overlying Upper Devonian to Lower Mississippian red beds of the Saint-Jules Formation (Jutras and Prichonnet 2002, 2004) (Figures 1, 2) by the Acadian unconformity, but it is not affected by the Acadian folding that affects the Silurian mudstone.

The Saint-Jogues-Sud and Huard faults (Figure 1) are thought to be among the faults that controlled sedimentation of the Saint-Jules Formation in the New-Carlisle area, located in the northwest sector of the Late Devonian to early Mississippian Paspébiac graben (Jutras and Prichonnet 2004). Away from the dyke swarm, the base of the Saint-Jules Formation is characterized by a petromictic conglomerate dominantly composed of calcareous

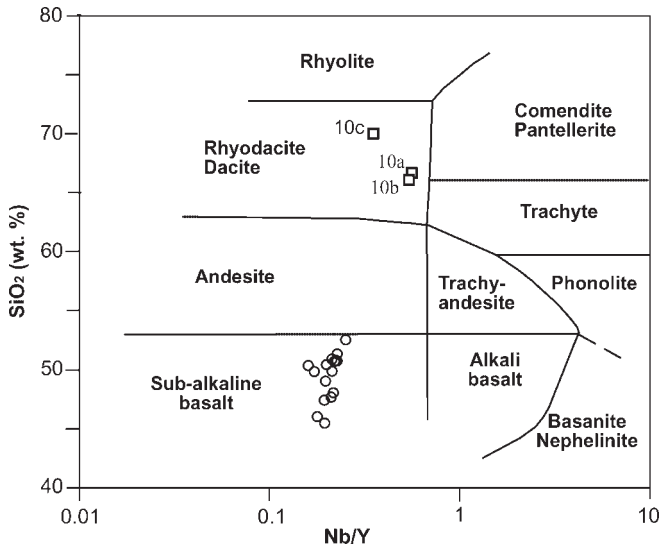

Figure 3. Plot of the New-Carlisle igneous bodies on a classification diagram based upon SiO_2–Nb/Y variations (after Winchester and Floyd 1977). Squares: dacite samples from locality 10 (Figure 1); circles: basalts from all other localities.

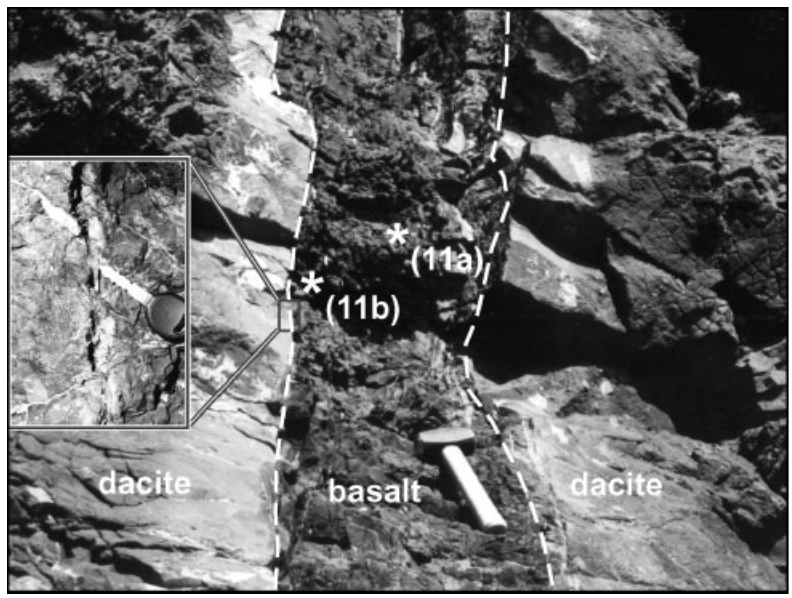

Figure 4. Mafic (basalt) dyke intruding a felsic (dacite) plug at New-Carlisle, with localities of samples 11a and 11b. Scale: Hammer is 26 cm. Inset shows an ankerite vein separating the mafic and felsic rocks. Scale: key is 7 cm.

sedimentary rock clasts. In the 50 m section that was measured in that basin, sandstones become increasingly dominant up the stratigraphy, whereas pedogenic calcretes are mainly found in the lower 15 m (Jutras and Prichonnet 2004).

The Saint-Jules Formation is the youngest unit to be affected by the basalt intrusions. It is unconformably overlain by polymictic conglomerates of the late Viséan Bonaventure Formation (Jutras *et al*. 2001) in the study area (Figures 1, 2).

3. ANALYTICAL METHODS

Mineral compositions of the aphanitic to porphyritic mafic rocks at New-Carlisle were determined on 24 samples from a combination of optical, X-ray diffraction and scanning-electron microscope (SEM) data obtained at the Université du Québec à Montréal (UQAM). Figure 1 shows the localities of the samples in Table 1, which reports semi-quantitative estimations of volumetric mineral contents derived from X-ray diffraction peaks.

Chemical compositions from core samples of 18 mafic dykes were determined with X-ray fluorescence (Philips PW2400 Spectrometer) at McGill University (Montréal) for major elements using fused beads prepared from ignited samples (Table 2). All samples are moderately to highly altered, as indicated by elevated loss-on-ignition (LOI) values ranging from 2.5 to 13.38% (Table 2). Total H_2O and CO_2 contents, which were determined by inductively coupled plasma–mass spectrometry (ICP-MS) at McGill University on six samples (Table 2), closely resemble LOI values and are therefore representative of total volatile contents. For plotting on variation diagrams, the analyses were recalculated to total 100% on a volatile (LOI)-free basis.

Stable isotope analysis of carbon and oxygen was done on 11 carbonate samples using a Multicarb preparation system and a dual inlet Isoprime mass spectrometer at UQAM (Table 3). Values are calibrated with the Vienna standards of the Peedee Belemnite (VPDB).

Rare earth element (REE) contents were determined at McGill University from instrumental neutron activation analysis (INAA) on five samples (Table 4). Values are normalized to C_1 chondrites for plotting (Cullers and Graf 1984).

4. MAFIC INTRUSIONS

Mafic dyke exposures at New-Carlisle are *c*. 20 m below to *c*. 5 m above the Acadian unconformity according to field measurements and cartographic extrapolations. The dykes are 0.5 to 30 m wide and strike north–south ($\pm 05°$). Bagdley (1956) referred to them as andesitic but did not provide geochemical data to support his classification. According to their SiO_2–Nb/Y content (Figure 3), they all classify as sub-alkaline basalt. They are, however, heterogeneous in terms of texture, ranging from aphanitic to strongly porphyritic. The groundmass is microcrystalline in all cases. The porphyritic material is also found in the form of nodules, up to more than 1 m in maximum diameter, in the largest, 30 m wide dyke at locality 13 (Figure 1).

Primary phases are not preserved in the mafic dykes. Instead of calcic plagioclase and pyroxene, they contain albite and/or anorthoclase, quartz, kaolinite, chlorite, apatite, and as much as over 25% Fe-Ti oxides (Table 1).

4.1. Alteration trends

The mafic rocks at New-Carlisle are cut by narrow (0.1 to 10 cm wide) ankerite veins that increase in abundance upwards toward the Acadian unconformity. The alteration trends defined below seem to be closely related to the density of this network of ankerite veins. For example, basaltic material taken near the contact with a 0.5 cm wide ankerite vein at locality 11 has higher albite contents (38 vol% in sample 11b) than material taken from the centre of the dyke (10% in sample 11a; sample localities are shown on Figure 4).

Aluminium and silicon are the only major elements that show relatively constant concentrations in the basalt samples (Table 2). Albitization is pervasive and, in some cases, quite penetrative. Many samples comprise more than 50% albite (Table 1) and can therefore classify as albitites. K-feldspars are dominant in one sample (4), which was taken at a lower level (*c*. 17 m below the unconformity) than most of the other samples and which is characterized by the presence of anorthoclase phenocrysts. K-feldspar concentrations tend to increase in samples taken more than 10 m below the unconformity (Figure 5a).

The alteration products of mafic minerals also change with depth. Iron and titanium oxides are most abundant near the unconformity (Figure 5b), whereas chlorite is only present deeper than 5 m below the unconformity (Figure 5c). Relatively fresh pyroxenes, amphiboles and biotite can mainly be found at depth, suggesting that

Table 1. Mineralogical compositions of rocks according to X-ray diffraction analysis

Sample	Depth from unconformity (m)	Quartz (vol%)	Albite (vol%)	K-feldspar (vol%)	Pyroxenes (vol%)	Amphiboles (vol%)	Biotite (vol%)	Apatite (vol%)	Hematite (vol%)	Anatase (vol%)	Rutile (vol%)	Kaolinite (vol%)	Chlorite (vol%)	Ankerite (vol%)	Calcite (vol%)
1	−2.5	4	37	11	—	—	8	1	6	6	—	3	—	22	1
2	−3.5	19	21	5	—	—	3	<1	8	3	—	13	—	22	1
3	−15	2	51	21	6	3	4	2	2	—	—	1	3	3	1
4	−17	4	—	61	1	—	2	—	<1	2	—	10	16	4	<1
5	−20	2	45	19	11	3	9	1	1	—	<1	1	6	2	—
6	−14	9	44	12	1	7	6	<1	1	1	<1	3	2	6	4
7	−10	4	59	10	<1	—	3	2	6	3	—	2	3	1	6
8	−8	6	53	13	2	—	3	2	5	4	—	3	3	5	1
9	−7	4	54	5	—	—	7	2	6	6	<1	3	2	7	5
10a	−1	37	22	13	1	—	7	—	<1	<1	—	8	—	10	<1
10b	−12	58	13	6	1	—	7	—	<1	<1	—	5	1	9	—
10c	−14	50	19	2	<1	—	—	—	<1	<1	—	1	—	10	—
11a	−12	17	10	18	<1	—	<1	1	5	1	—	17	17	8	5
11b	−12	18	38	4	1	—	1	1	2	2	—	17	12	6	<1
12a	−5.5	18	33	8	—	—	1	3	7	7	<1	7	—	25	—
12b	1	3	39	11	—	—	3	3	13	13	1	4	—	10	3
13a	−5	3	68	2	<1	—	1	<1	6	3	<1	3	—	10	2
13b	−1	<1	75		—	—	2	—	8	3	—	1	—	9	2
14	−5	11	48	12	<1	—	1	2	7	6	—	—	—	8	—
16a	−4.5	10	43	8	2	—	1	2	10	4	—	5	—	16	—
16b	2	5	57	11	—	—	<1	—	13	5	—	5	—	4	—
17a	−5.5	7	55	6	3	—	<1	3	3	6	<1	3	—	15	1
17b	−0.5	15	32	5	1	—	3	3	6	3	<1	10	—	2	20
18a	−3	11	56	5	3	—	2	2	6	4	—	3	—	8	<1
18b	1	4	36	12	—	—	1	—	2	4	2	6	—	32	2
19	−2	20	33	7	<1	—	—	<1	6	2	—	3	—	4	23
20	0	9	19	11	1	—	2	1	11	8	—	14	—	20	5
C1	−5	10	2	—	—	—	<1	—	—	—	—	—	—	85	3
C2	−5	1	1	—	—	—	2	—	—	—	—	2	—	82	9
C3	1	5	—	<1	—	—	<1	—	2	—	—	<1	<1	79	13
C4	1	9	—	4	—	—	2	<1	—	—	—	<1	—	73	10
C5	1	13	1	—	—	—	2	—	—	—	—	2	—	73	6
C6	1	21	—	1	—	—	<1	1	—	—	<1	2	—	58	16
C7a	1	4	<1	<1	—	—	2	—	—	—	—	<1	—	5	86
C7b	1	20	1	2	—	—	—	<1	1	—	—	1	<1	28	44
C7c	1	16	1	4	—	—	<1	2	—	—	—	1	1	66	8
C8	1	22	<1	<1	—	—	—	—	—	—	—	1	<1	5	68
C9	14	<1	—	—	—	—	—	<1	—	—	<1	—	—	<1	99
FS1	1	26	<1	11	—	—	3	—	—	—	6	5	—	39	8
FS2	1	30	19	17	—	—	2	—	2	<1	4	3	—	19	4
FS3	5	21	<1	6	<1	—	3	—	2	—	4	5	—	—	58
FS4	1	19	13	16	—	—	3	—	2	—	10	4	—	24	10
SS1	40	15	—	2	—	—	—	—	—	—	—	2	—	—	78

Samples 1–9 and 11–20: mafic rocks (localities shown on Figure 1); samples 10a–c: dacite plug (locality shown on Figure 1). samples C1–C9: carbonate; samples FS1–FS4: fluidized sands; sample SS1: Saint-Jules Formation sandstone.

Table 2. Chemical composition of rocks according to X-ray fluorescence analysis

Sample	Depth from unconformity (m)	SiO_2 (wt%)	TiO_2 (wt%)	Na_2O (wt%)	K_2O (wt%)	Al_2O_3 (wt%)	Fe_2O_3 (wt%)	MnO (wt%)	MgO (wt%)	CaO (wt%)	P_2O_5 (wt%)	LOI (wt%)	Total (wt%)	H_2O+CO_2 (wt%)
1	−2.5	41.49	3.12	4.07	2.91	16.67	11.09	0.128	2.95	7.06	0.713	10.53	100.8	
2	−3.5	43.66	3.414	1.4	0.84	14.42	12	0.177	3.07	7.21	1.348	12.93	100.51	
3	−15	47.86	3.598	4.52	2.15	14.01	14.33	0.248	3.77	5.94	1.264	2.6	100.38	3
4	−17	49.52	2.615	4.37	2.31	16.44	11.28	0.286	4.58	6.41	0.505	2.5	100.95	2.39
5	−20	48.31	3.56	5.18	1.11	13.47	13.84	0.275	4.16	6.27	1.278	2.79	100.29	
6	−14	47.35	2.919	3.96	2.73	16.28	12	0.141	3.24	5.02	0.545	6.12	100.39	5.94
7	−10	44.87	3.83	4.33	2.75	15.04	15.57	0.194	1.21	5.6	1.328	5.94	100.75	
8	−8	45.01	2.959	4.98	1.62	13.84	14.79	0.16	4.29	4.81	1.329	6.83	100.67	
9	−7	44.74	3.168	4.8	2.28	14.35	14.86	0.12	2.66	5.31	1.423	6.72	100.51	
10a	−1	60.62	0.6	1.46	3.05	12.85	4.51	0.056	2.63	5	0.118	9.45	100.41	9.35
10b	−12	60.45	0.588	1.82	3.03	13.11	4.46	0.063	2.84	4.77	0.131	8.9	100.23	8.69
10c	−14	63.99	0.533	3.2	1.6	10.52	2.63	0.069	2.87	5.67	0.123	8.91	100.17	9.02
11a	−12	43.45	3.461	2.31	2.1	14.39	13	0.23	2.31	8.05	1.383	10.13	100.86	10.28
12a	−5.5	40.32	3.982	3.66	2.8	15.01	9.19	0.121	3.98	8.05	1.449	11.48	100.15	
13a	−5	47.14	1.69	6.6	1.19	16.06	13.77	0.139	2.46	4.61	0.741	6.57	101.01	6.58
14	−5	48.3	3.124	6.34	0.6	14.55	12.01	0.078	2.22	5.63	1.489	6.64	101.01	
16a	−4.5	46.01	2.835	3.62	2.6	14	10.68	0.096	3.03	6.61	1.304	9.27	100.1	
17a	−5.5	45.39	2.374	5.44	2.13	14.93	5.42	0.106	3.48	8.8	1.38	11.01	100.5	11.13
18a	−3	47.53	2.103	5.04	2.66	16.8	11.7	0.065	1.92	4.79	1.141	6.47	100.26	
19	−2	46.54	1.927	3.83	2.63	14.27	5.75	0.079	2.66	9.95	0.88	11.83	100.41	
20	0	40.09	2.688	1.82	2.79	16.07	9.69	0.12	3.57	9.15	1.275	13.38	100.69	

Total iron present has been recalculated as Fe_2O_3. Detection limits are based on three times the background sigma values.
Samples 10a–c: dacite plug; all other samples: mafic dykes.

Table 3. Stable isotopes of carbon and oxygen according to mass spectrometry analysis

Sample	$\delta^{13}C$ (VPDB)	$\delta^{18}O$ (VPDB)
C1	−4.80	−11.29
C2	−4.02	−10.61
C3	0.43	−10.91
C4	−1.79	−10.69
C5	−0.35	−10.85
C6	−1.21	−9.91
C7a	−2.29	−7.65
C7b	−1.82	−9.10
C7c	−2.37	−10.93
C8	−1.84	−6.13
C9	−1.88	−7.55

Calibrated with the Vienna standards of the Pee Dee Belemnite (VPDB). C1–2: ankerite veins in dyke 13; C3–6 and C7c: carbonate melt; C7a and C8–9: pedogenic calcretes.

the alteration of mafic minerals was altogether more pervasive near the unconformity, where the ankerite veins are most abundant. More extensive alteration near or above the Acadian unconformity is also indicated by a decrease of LOI values with increasing depth from the unconformity (Figure 5d).

The least altered samples (LOI $<$ 7%) show a decrease in $CaO/(Na_2O+K_2O)$ ratios up towards the Acadian unconformity (Figure 5e), even though this relationship is partly obscured by an increase in carbonate contamination in the same direction (Figure 5f). It should be noted that, of the six basalt samples that were analysed for their

Table 4. Rare earth element contents according to instrumental neutron activation analysis

Sample	La (ppm)	Ce (ppm)	Nd (ppm)	Sm (ppm)	Eu (ppm)	Tb (ppm)	Yb (ppm)	Lu (ppm)
13a	23	56.7	33	9	2.22	1.36	3.8	0.6
C1	8	3.385	7.16	1.1	0.488	0.183	0.35	0.07
C3	12.2	29.121	14.6	3.5	0.818	0.545	1.18	0.16
FS1	22.8	34.617	18.75	4.1	0.854	0.576	1.75	0.253
SS1	19.55	42.817	20.3	3.65	0.768	0.58	2.08	0.308

C1, Ankerite vein in dyke 13; C3, carbonate melt in peperite; FS1, fluidized sand dyke; SS1, undisturbed sandstone of the Saint-Jules Formation. Values are calibrated to C1 chondrites.

total CO_2 and H_2O contents, only the samples taken from more than 10 m below the unconformity (samples 3, 4 and 6) show sufficient CaO to balance their CO_2 content if the latter was associated with calcite only (Table 2). The Ca contents of samples 11a, 13a and 17a account for only 87.8%, 73.1% and 69.8% of the total CO_2 content of these samples (respectively), if all of it was involved in the formation of calcite (Table 2). Hence, the mafic rocks are virtually depleted in Ca near the unconformity.

5. PEPERITES

The basal beds of the Saint-Jules Formation, 15 to 20 km east of New-Carlisle, comprise red fanglomerates that are almost exclusively composed of poorly rounded calcareous clastic rock clasts derived from the local Silurian Chaleurs Group (Jutras and Prichonnet 2004). In the vicinity of the mafic dyke swarm at New-Carlisle, these beds were involved in the formation of peperite, as they are invaded by blocky clasts of partly devitrified mafic glass and porphyritic basalt (Figure 6a) that commonly show the typical jigsaw-fit of juvenile clasts (Figure 6b, c), a characteristic feature of most blocky peperites (Hanson and Schweickert 1982; Busby-Spera and White 1987; Branney and Suthren 1988; Boulter 1993; Goto and McPhie 1996; Dadd and Wagoner 2002; Skilling *et al*. 2002; Squire and McPhie 2002). Mingling of glassy and non-glassy clasts is also commonly observed in other peperites, although the two types of clasts are thought to form at different stages of peperite formation (Hanson and Schweickert 1982; Skilling *et al*. 2002). The New-Carlisle peperites also show evidence of melting, a far less common feature that has been documented in only a few examples (Schminke 1967; Ito *et al*. 1984; Krynauw *et al*. 1988; Yamamoto *et al*. 1991; McPhie and Hunns 1995; WoldeGabriel *et al*. 1999; Martin and White 2002).

Because the Acadian unconformity dips westward and eastward from the New-Carlisle inlier (Figures 1 and 7), exposure of the basal peperite pinches out towards the inlier due to erosion, and eventually disappears below sea-level away from it. The 20 dyke localities are indicated from west to east on Figure 1, and the peperite facies associated with each of these localities are described below.

5.1. Localities 1 to 11

Surface exposures at dyke localities 1 to 11 are below the level of the Acadian unconformity. Hence, basal post-Acadian peperites cannot be observed directly above the dykes at these localities. However, a small 2-m-thick wedge of Saint-Jules Formation clastic rocks can be observed unconformably below the Bonaventure Formation near dyke localities 1 and 2 on the west side of the New-Carlisle inlier. The succession consists of 0.5 m of red, granular conglomerate overlain by 1.5 m of pebbly sandstone with pedogenic calcrete nodules (Jutras and Prichonnet 2004). Gravel composition is similar to that of the Saint-Jules Formation throughout the Paspébiac graben, including only locally derived clasts from the Silurian Chaleurs Group succession, which is dominated by calcareous sedimentary rocks. Apart from the presence of a sandstone dyke near the mafic dyke of locality 1, these clastic rocks are seemingly undisturbed. This sandstone dyke extends down into the Silurian basement for about 1 m before the outcrop exposure is lost. It cross-cuts the overlying Saint-Jules Formation above the Acadian

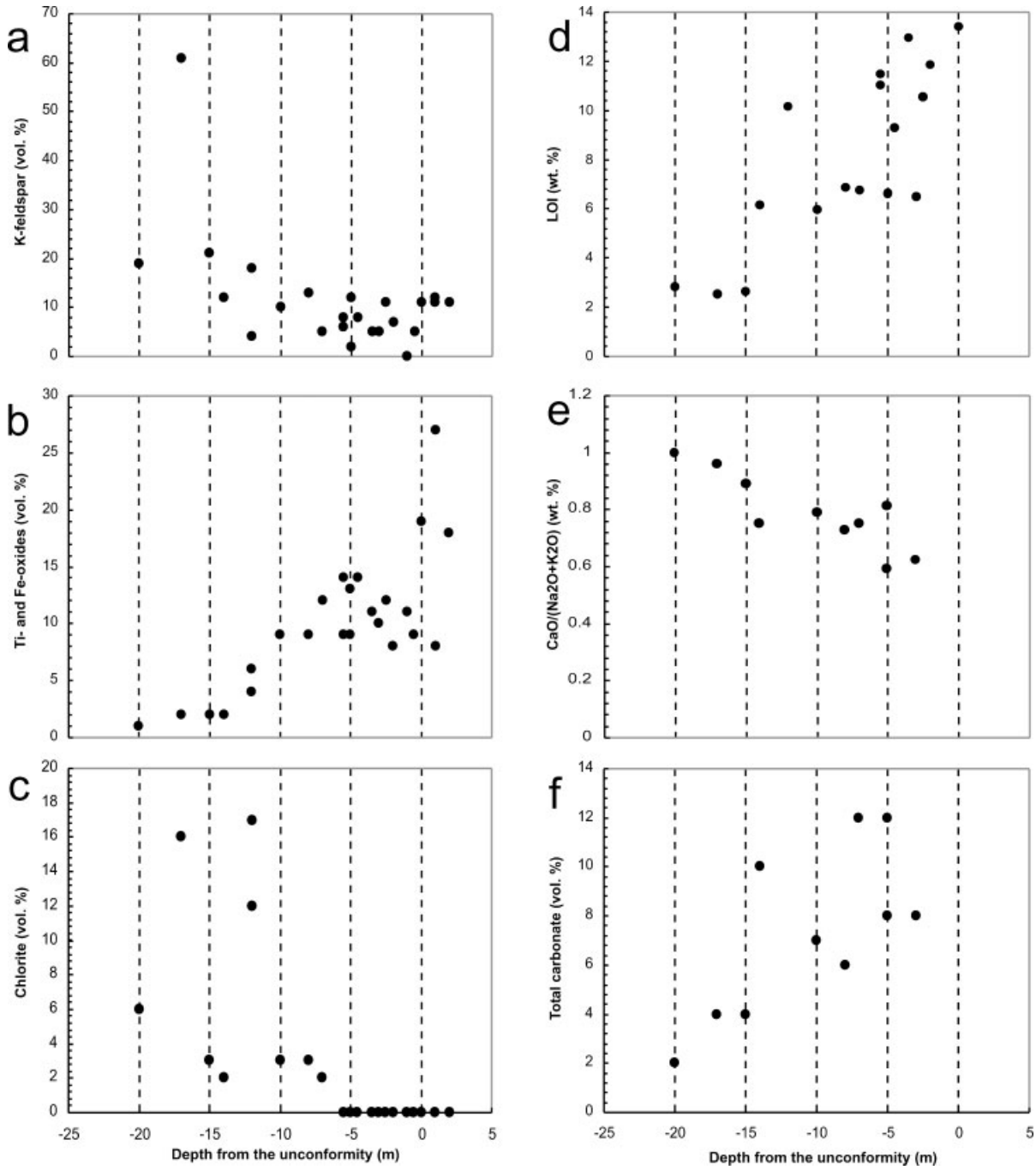

Figure 5. Distribution of (**a**) K-feldspar, (**b**) Ti-Fe oxides, (**c**) chlorite, (**d**) loss-on-ignition values (LOI), (**e**) $CaO/(Na_2O + K_2O)$ ratios, and (**f**) total carbonate in relation to the measured or estimated depth at which the mafic samples were taken with respect to the Acadian unconformity.

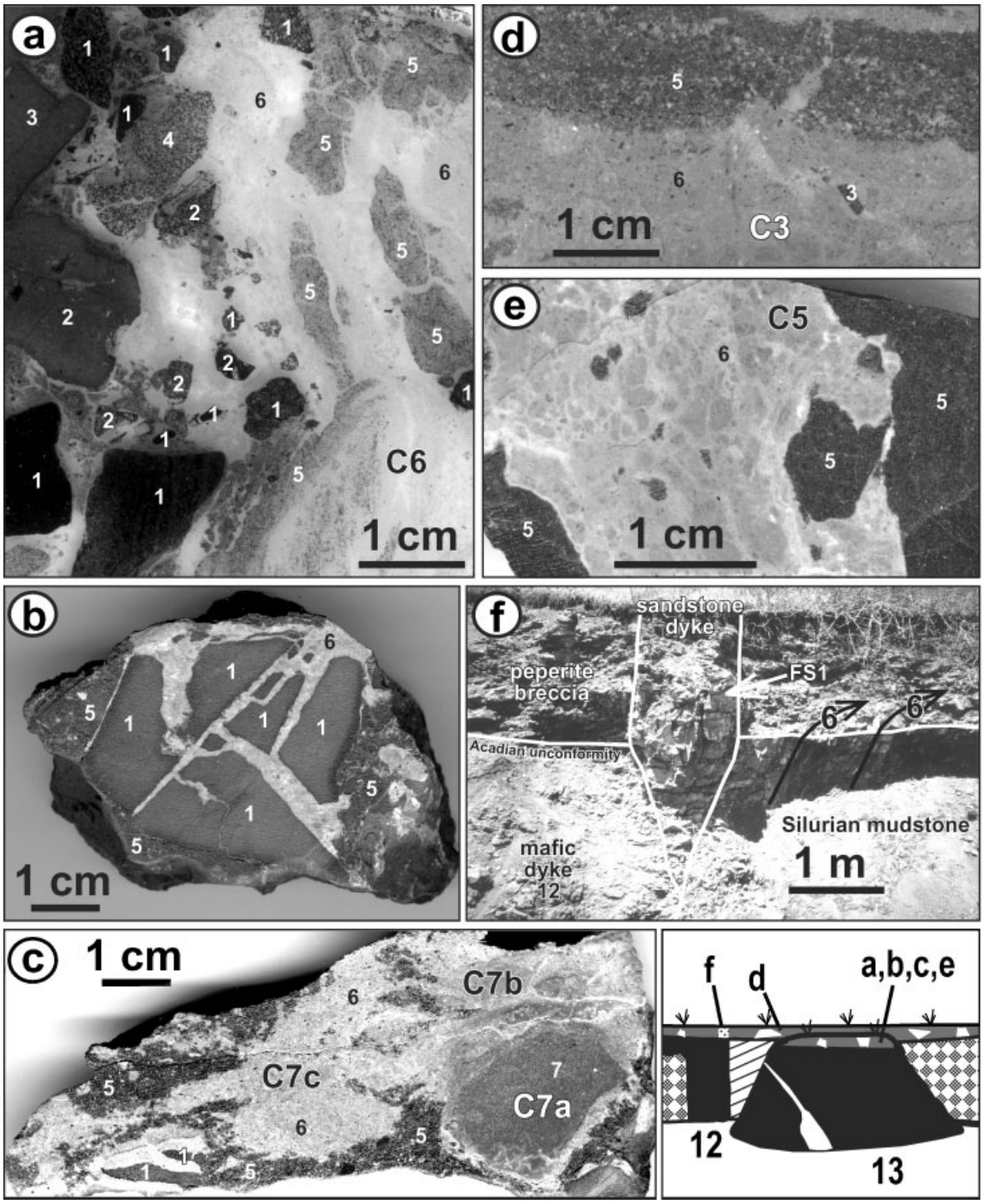

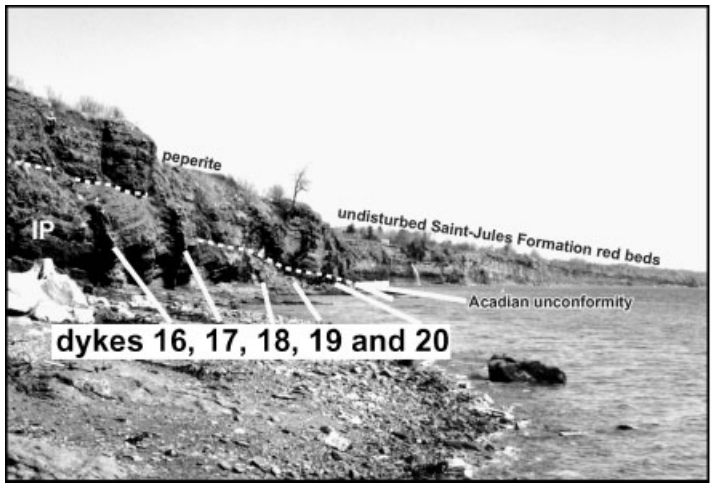

Figure 7. General view of the post-Acadian peperite, evolving laterally into undisturbed clastic sediments of the Saint-Jules Formation and tilting away from the New-Carlisle inlier. The dykes can be seen as salients along the coastal cliff. Height of cliff *c.* 20 metres.

unconformity (Middle Devonian), and is sharply truncated by the overlying Bonaventure Formation (late Viséan) at the level of a minor Carboniferous unconformity (Figure 8). The latter unit includes abundant, round clasts of mafic and ankeritic material in its lowermost conglomerates, along with reworked sandstone clasts of the Saint-Jules Formation (Jutras and Prichonnet 2004). Finally, it is noteworthy that the dyke at locality 2 terminates before reaching the Acadian unconformity.

5.2. Localities 12 and 13

A diffuse contact between tightly veined basalt and peperite is observed at the level of the Acadian unconformity at localities 12 and 13. The bulk of the first 1.5 m of peperite (the rest is unexposed) is massive micritic carbonate (*c.* 60% of the peperite volume) and a mixture of siliciclastic grains, clays and oxides (*c.* 25–30%). These two matrices do not intermix and are mainly in fluidal (Figure 6c, d) or globular (Figure 6e) contact with each other, although fragments of the siliciclastic–oxide material are also observed within the ankerite (Figure 6a, e). The micritic carbonate matrix is mainly composed of ankerite (79%, with 13% calcite, 5% quartz, 2% hematite, and traces of feldspar, micas, kaolinite and chlorite in sample C3; Table 1).

Floating in this bimodal matrix are juvenile clasts (glassy fragments and porphyritic basalt; *c.* 10%) with abundant jigsaw-fits (Figure 6b, c), and sub-rounded gravel-size clasts of non-calcareous sedimentary rocks and dacite (*c.* 0–5%) (Figure 6a). However, the limestone and calcareous mudstone clasts that form the bulk of the Saint-Jules Formation are absent in this peperite facies. In the nomenclature proposed by Hanson and Wilson (1993), this peperite facies is characterized by a 'dispersed' texture, juvenile clasts occupying less than 50% of the volume.

Figure 6. Peperite associated with the dykes at localities 12 and 13 (refer to Figure 1 for localities). (**a**) Mingling of juvenile clasts and non-calcareous sedimentary rock clasts in a bimodal matrix of carbonate (sample C6) and siliciclastic–oxide material. (**b**) Jigsaw-fit juvenile clasts within the peperite. (**c**) Pebble-size calcrete fragment (sample C7a), partly digested (sample C7b) and incorporated in the carbonate matrix (sample C7c) of the peperite. Jigsaw-fit juvenile clasts are also visible on the left. (**d**) Fluidal contact between bands of carbonate (sample C3) and siliciclastic–oxide material in the peperite. (**e**) Pocket of carbonate (sample C5) within siliciclastic–oxide material. Note that the contacts are mainly globular or fluidal, although some blocky clasts of siliciclastic–oxide material are incorporated within the carbonate. (**f**) Large sandstone dyke on the eastern margin of the dyke at locality 12. Bands of ankerite extend from the Silurian basement into the post-Acadian peperite, in which they curve towards the horizontal. Localities are shown on the inset (see legend of Figure 1). Key: 1, partly devitrified glassy fragments; 2, porphyritic juvenile clasts; 3, mudstone clast with a reaction rim; 4, disintegrated sandstone clast; 5, siliciclastic–oxide material; 6, carbonate matrix.

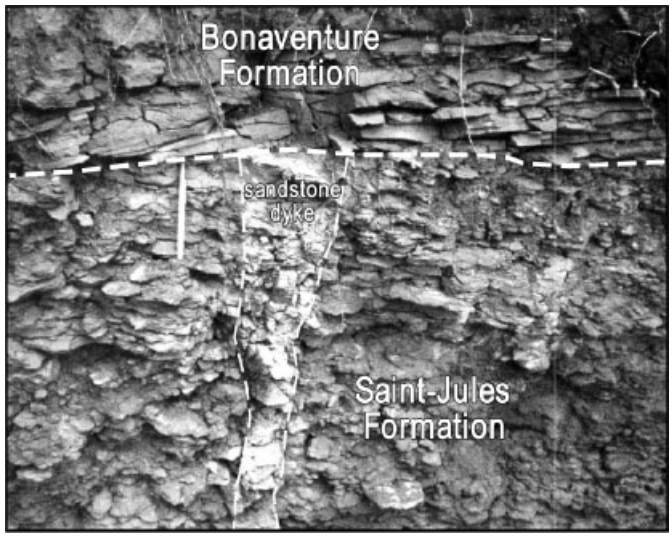

Figure 8. Truncation of a sandstone dyke at the contact between the Saint-Jules and Bonaventure formations on the west side of the New-Carlisle inlier. Scale: pen is 15 cm.

A pedogenic calcrete hardpan is partly preserved *c*. 1 m above the diffuse contact between basalt and peperite at locality 13. The calcrete merges laterally with the carbonate matrix of the peperite, leaving but a few incompletely digested clasts (Figure 6c).

A large vein separating basement rocks from the east side of the dyke at locality 12, which is separated from the dyke at locality 13 by only 5 m of basement rocks, evolves upward into a 1-m-wide sandstone dyke that truncates the peperite above the unconformity (Figure 6f). The sandstone dyke is nearly 50% carbonate, mainly ankerite, with high contents of feldspars (12%) and rutile (6%) (sample FS1 in Table 1; sampling locality shown on Figure 6f). On the east side of the sandstone dyke, 5- to 10-cm-thick bands of ankerite curve and diffuse away from it (Figure 6f). Their orientation evolves from nearly vertical near the dyke to horizontal a few metres away from it.

5.3. Localities 14 to 20

The peperite above the dykes at localities 14 and 15 is exposed but inaccessible. The basal peperite breccia at localities 16 to 20 is massive, but internally shows a high lateral variability. Gravel-size clasts form the bulk of the peperite in some areas, but are dispersed within sandy matrix in other areas. It was also noted that blocky juvenile clasts are mainly concentrated either directly above each dyke, or immediately to the east of them. On average, sub-angular gravel-size basalt clasts (*c*. 5–50% of the peperite volume) and sub-rounded calcareous sedimentary rock clasts (*c*. 30–40%) form the bulk of the material, but many of the latter type of clasts are thoroughly metamorphosed to hornfels or show a reaction rim of contact metamorphism (Figure 9h), features that are not observed in Saint-Jules Formation sediments away from the dyke swarm. Sub-angular glassy fragments (1–3%) and sub-rounded non-calcareous sedimentary rock clasts (1–2%) form the rest of the peperite framework. The finer fraction (10–50%) is mainly composed of hematite- and rutile-coated sand, partly clast-supported and partly floating in calcite cement.

Massive sandstone layers appear east of the dyke at locality 17 within the peperite breccia. They diffusively pinch out to the west and thicken eastward until they disappear below sea-level. They intrude structureless peperite breccia, thickening upward into it in some areas (Figure 9m), and feeding sandstone dykes (Figure 9d). Because of the absence of sedimentary structures or fabric in these sandstones, which are partly floating in calcite and show evidence of plastic flow (Figure 9m), they are interpreted as fluidized sediments and are therefore considered to be

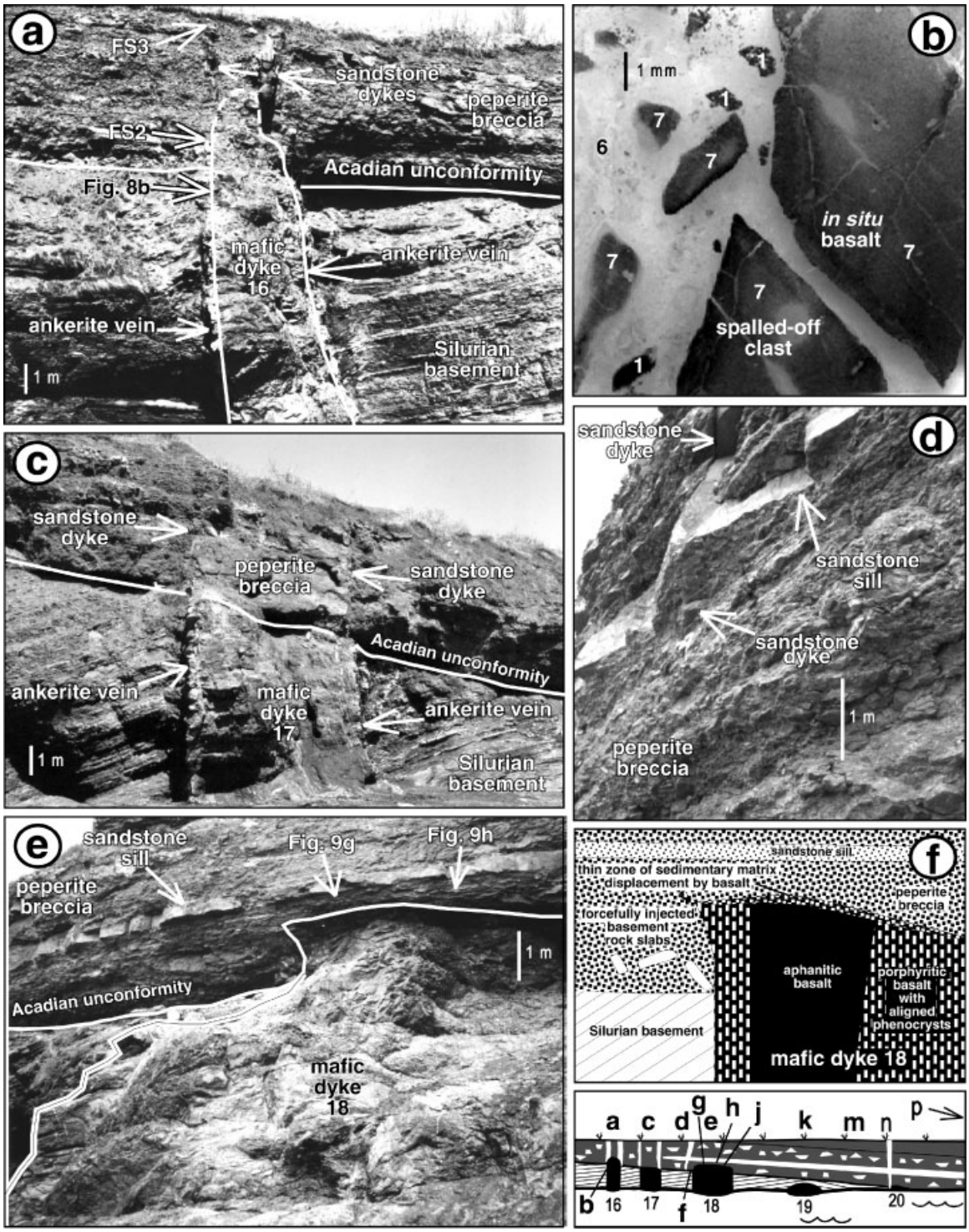

Figure 9. Continued.

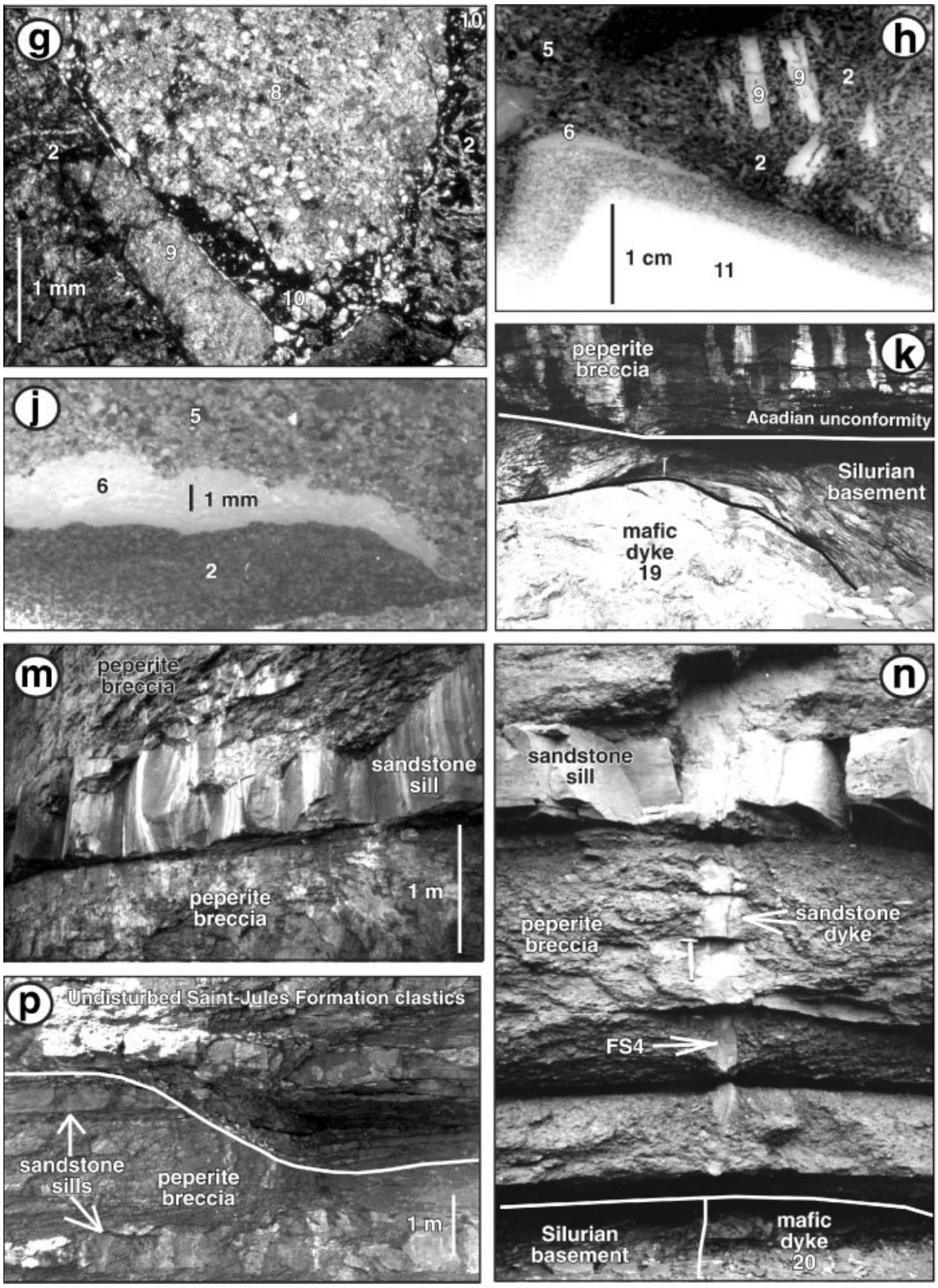

part of the peperite. To differentiate them from across-strike 'sandstone dykes', these along-strike fluidized sands are here referred to as 'sandstone sills'. Such stratification of peperitic material has been reported elsewhere (Brooks *et al.* 1982; Branney and Suthren 1988; Brooks 1995; Doyle 2000).

East of the dyke at locality 20, the succession of peperite breccia and sandstone sills is *c*. 12 m thick. It abruptly abuts against and bends an otherwise undisturbed sedimentary succession of the Saint-Jules Formation (Figure 9p), *c*. 100 m east of the dyke at locality 20. East of this lateral contact, the succession shows trough cross-bedding and abundant calcrete nodules, which are typical of the Saint-Jules Formation away from the New-Carlisle dyke swarm (Jutras and Prichonnet 2004).

The dyke at locality 16 is only 2 m wide and is the narrowest of those exposed at the level of the unconformity (i.e. localities 12–20). It is also the one that extends highest above the unconformity (2 to 3 m), before grading into peperite (Figure 9a). On each side of this dyke, vertical ankerite veins separate it from the Silurian basement and evolve into sandstone dykes above the unconformity (Figure 9a). These ankerite veins contain juvenile clasts spalled-off from the mafic dyke (Figure 9b), and the sandstone dyke that evolves upward from it includes high contents of feldspar (36%) and rutile (4%) 1 m above the Acadian unconformity (sample FS2; sampling spot shown on Figure 9a). Four metres higher in the same sandstone dyke (sample FS3; sampling spot shown on Figure 9a), the feldspar content is only 7%, but the rutile content remains high (4%). The composition of the carbonate matrix also changes vertically. For example, sample FS2 contains 19% ankerite but only 4% calcite, whereas sample FS3, collected 4 m higher in the same sandstone dyke, contains no ankerite but 58% calcite. It is noteworthy that undisturbed sandstone of the Saint-Jules Formation, a few kilometres to the east, contains only 2% feldspar, no ankerite and no rutile (sample SS1 in Table 1).

The 10-m-wide dyke at locality 17 does not extend above the unconformity, but it is also bound on each side by carbonate veins that evolve upward into sandstone dykes above the unconformity (Figure 9c). The 15-m-wide dyke at locality 18 sharply intrudes the peperite for the first 1 m above the unconformity (Figure 9e). Boulder-size slabs of Silurian basement rocks are present in the first metre of peperite, adjacent to the igneous body (Figure 9f). A diffuse contact between basalt and highly oxidized clastic material can be observed at the dyke–peperite contact, where basalt displaced part of the sedimentary matrix (Figure 9f, g). Such displacement of sedimentary matrix by igneous material was observed by Boulter (1993), which he associated with fluidization of the finer fraction of the host sediment. However, most of the original contact between basalt and sedimentary rock clasts, which form a weak zone with discontinuous remnants of intervening sedimentary matrix (Figure 9g), were apparently affected by subsequent reworking and can best be observed in abundant composite clasts within the peperite that shows the welded contact between basalt and clastic material. For example, Figure 9h shows a sub-rounded clast of mudstone, metamorphosed around its rim and still partly welded to basalt. Note that ankerite, which is diffusively coating the top of many clasts within the peperite (Figure 9j), coats the welded clast of Figure 9h, but does not extend within the suture zone. Finally, injection of sediments in minute fractures of the basalt is common at the top of the dyke at locality 18, which is observed at many igneous rock–peperite contacts and is associated with the fluidization of sediments (Kokelaar 1982, 1986; Busby-Spera and White 1987; Goto and McPhie 1996; Doyle 2000).

Figure 9. Peperite associated with the dykes at localities 16–20. (**a**) Intrusion of the dyke at locality 16, and associated sandstone dykes (samples FS1 and FS2) within post-Acadian peperite breccia. (**b**) Incorporation of juvenile clasts within an ankerite vein siding the dyke at locality 16. (**c**) Truncation of the dyke at locality 17 by post-Acadian peperite breccia, and truncation of the latter by sandstone dykes. (**d**) Sandstone dykes sourced from a sandstone sill. (**e**) Partial intrusion of a dyke within post-Acadian peperite breccia at locality 18. (**f**) Large basement slabs that were seemingly injected within the post-Acadian peperite breccia on the west side of the dyke at locality 18. (**g**) Sedimentary matrix replaced by basalt at the contact between the dyke at locality 18 and the post-Acadian peperite breccia. (**h**) Sub-rounded calcareous mudstone clast welded to basalt and incorporated as a composite clast within the peperite breccia above the dyke at locality 18. (**j**) Ankerite diffusing from a juvenile clast in the peperite breccia above the dyke at locality 18. (**k**) Top of the dyke at locality 19, which terminates less than 1 m below the Acadian unconformity. Scale: hammer is 26 cm. (**m**) Irregular upper contact between a sandstone sill and peperite breccia. (**n**) Sandstone dyke (sample FS4) issued from the west side of the dyke at locality 20 and diffusing within peperite breccia and a sandstone sill. Scale: hammer is 26 cm. (**p**) Sandstone sill and peperite breccia abutting and gently folding otherwise undisturbed clastic rocks of the Saint-Jules Formation, approximately 100 m east of the dyke at locality 20. Localities are shown on the inset (see legend of Figure 1). For key to numbers 1–6, see caption of Figure 6; 7, microcrystalline basalt; 8, sandstone granule; 9, albite phenocryst; 10, hematite-coated clastic material infiltrating along the contact between basalt and the sandstone granule; 11, calcareous mudstone clast with a reaction rim.

The 5-m-wide dyke at locality 19 terminates less than 1 m below the Acadian unconformity at the site of the exposure (Figure 9k). However, the overlying peperitic material is similar to that at localities 14 to 20, except that it includes fewer juvenile clasts and sedimentary rock clasts with reaction rims.

Only the upper 10 cm of the western side of the dyke at locality 20 is exposed (Figure 9n), whereas the rest of it disappears to the east below sea-level along with the Acadian unconformity (Figure 1; locality sketch). An ankerite vein beside the dyke evolves upward into a sandstone dyke with abundant feldspar (29%), rutile (10%) and ankerite (24%) (cf. sample FS4, taken near the base of the sandstone dyke; Table 1, Figure 9n) above the Acadian unconformity. This sandstone dyke diffuses through the sandstone sills that intrude the coarse peperite (Figure 9n).

6. CARBONATE GEOCHEMISTRY

6.1. Stable isotopes of carbon and oxygen

Various samples of carbonate material were analysed for carbon and oxygen isotopes at locality 13 (Figures 1 and 10; Table 3). They include pedogenic calcretes (samples C7a and C8), ankerite veins within the mafic body (samples C1 and C2, respectively taken 5 and 4 m below the Acadian unconformity), and the ankeritic bulk of the overlying peperite mass (samples C3–C6, and C7c). Another calcrete sample (C9) was taken from a hardpan within the undisturbed Saint-Jules succession that lies to the east of New-Carlisle. It shows similar stable isotope values as the two samples of the previously mentioned calcrete remnant that sits *c*. 1 m above the dyke at locality 13, and which laterally merges with the carbonate matrix of the peperite. Sample C8 was taken from a well-preserved part of this calcrete, whereas sample C7a was taken from the interior of a partly preserved clast of the calcrete within the carbonate matrix. The clast is partially digested around its edge (sample C7b) and diffuses into the surrounding carbonate matrix (sample C7c) (Figure 6c). Whereas δ^{13}C values remain relatively constant (about −2), independent of the degree of calcrete integrity, increasingly light δ^{18}O values are observed with an increasing degree of calcrete disintegration (from −10.93 to −7.65 in samples C7a–c on Figures 6c and 10).

Excluding the mixed isotopic composition of sample C7b, the three groups of samples show three well-defined distribution patterns (Figure 10). The ankerite veins below the unconformity have light δ^{18}O values (−11.29 to

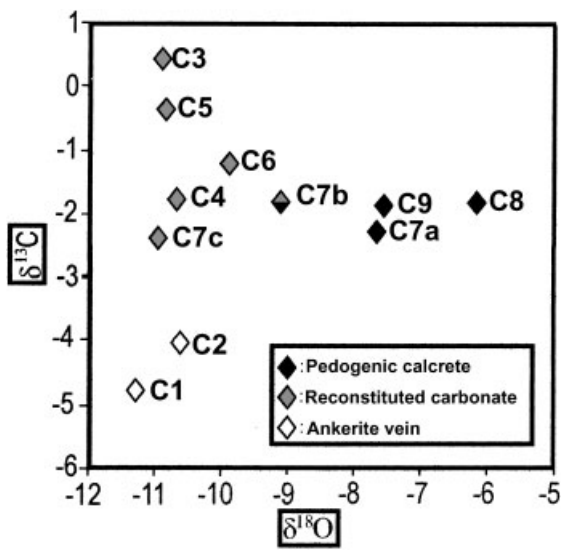

Figure 10. Carbon and oxygen isotopic ratios in ankerite veins within the dyke at locality 13 (samples C1–2), the carbonate matrix in the overlying peperite (samples C3–6 and C7c), and in pedogenic calcrete remnants of the Saint-Jules Formation (samples C7a and C8–9).

−10.61) and light δ^{13}C values (−4.80 to −4.02), whereas the carbonate matrix of the peperite has light δ^{18}O values (−10.91 to −9.91) and heavy δ^{13}C values (−2.37 to 0.43). In contrast to both ankerite vein and peperite matrix samples, the calcretes have δ^{18}O values that are less light (−7.65 to −6.13), with moderately heavy δ^{13}C values (−2.29 to −1.84) (Figure 10).

6.2. *Rare earth elements (REE) analysis*

The ankerite vein of sample C1, taken in the middle of the 30-m-wide mafic dyke at locality 13, shows a distinctive distribution of rare earth elements, with low concentrations, a strong negative Ce anomaly and a positive Eu anomaly (Figure 11). This is in marked contrast to the high REE concentrations of its host basalt, which shows a small positive Ce anomaly and a negative Eu anomaly. The sub-unconformity ankerite vein (C1) also contrasts greatly with the mineralogically similar carbonate matrix in the overlying peperite, which is richer in rare earth elements and shows a weak positive Ce anomaly and a negative Eu anomaly (sample C3 in Figure 11). The REE pattern of the carbonate matrix closely resembles that of undisturbed calcareous muddy sandstone of the Saint-Jules Formation (sample SS1) (Figure 11) near the town of Paspébiac (Figure 1). Finally, a sample of sandstone dyke (sample FS1) in the peperite shows a slight negative Ce anomaly and a smaller negative Eu anomaly, but similar REE concentrations as the undisturbed calcareous muddy sandstone (sample SS1) (Figure 11).

7. DISCUSSION

7.1. *Rapid cooling and quenching of the New-Carlisle dykes at the Acadian unconformity*

High porosity and water content in the sub-unconformity regolith may have restricted magmatic ascent in the basalt dykes at localities 2 and 19 (Figures 1 and 8c) by promoting a sudden decrease in magma temperature and a sudden increase in viscosity. There is nothing about the size or the texture of these two dykes that would explain why their ascent ceased at a lower level than the others. We hypothesize that they might be among the first dykes to be emplaced, and thus would have encountered a colder environment than subsequent dykes. For most of the other dykes, more drastic changes in porosity and associated water contents were necessary to stop the course of the rising melts, which only occurred when the latter reached the poorly consolidated upper Palaeozoic sediments above the unconformity (Figure 12a).

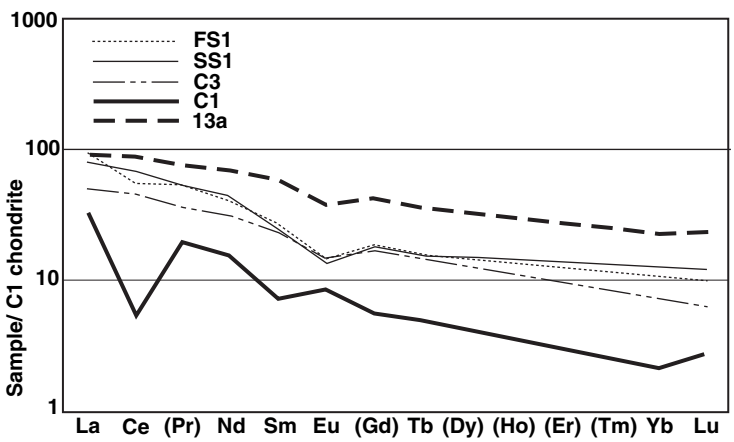

Figure 11. Rare earth element content of the dyke at locality 13 (sample 13a), an ankerite vein within the dyke (C1), carbonate matrix in the peperite above the dyke (C3), a sandstone dyke connecting to the dyke at locality 12 (FS1), and undisturbed sandstone of the Saint-Jules Formation near the town of Paspébiac (SS1).

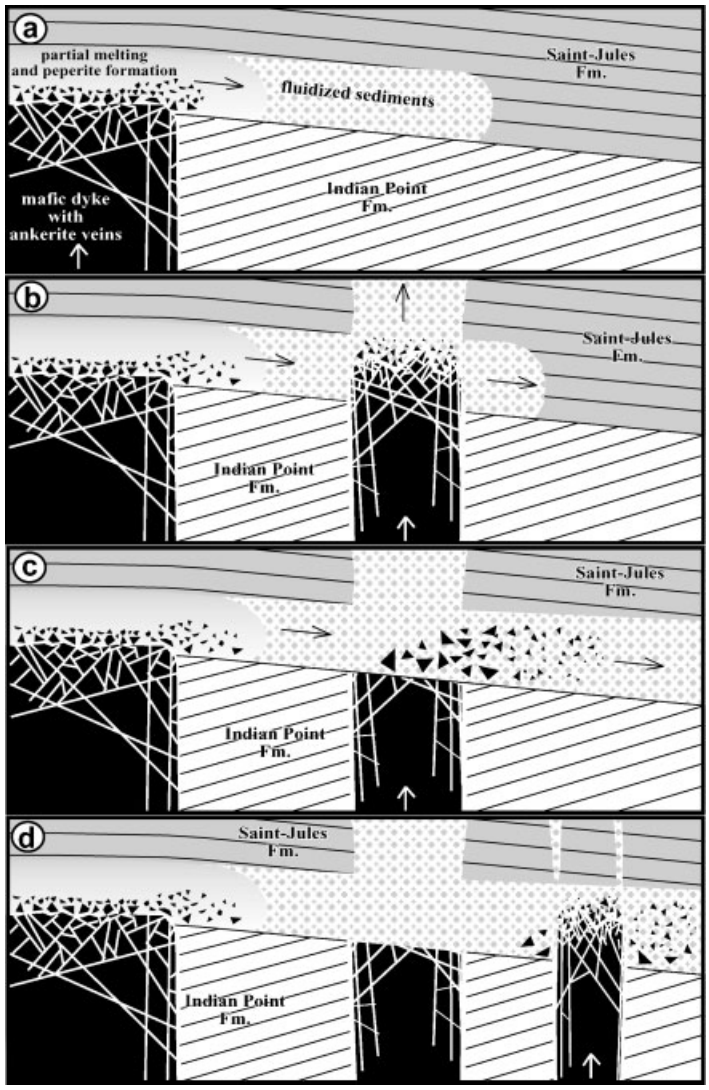

Figure 12. Proposed model for the formation of ferrocarbonatite and peperite during dyke emplacement at New-Carlisle. (**a**) Emplacement of the large dyke at locality 13, stopping its course abruptly at the Acadian unconformity, where porous clastic sediments and underlying regolith are engorged with cold water at shallow burial depth. Uplift, invasion of carbonated fluids from veins within the dyke, melting of calcareous clastic rocks, and formation of abundant juvenile clasts occur as a result. The carbonate melts flow down the slope developed on the unconformable surface due to their lack of buoyancy with respect to the overlying groundwater column. (**b**) Subsequent dyke emplacements experience a less drastic change in temperature and are able to extend higher into the post-Acadian sedimentary basin deposits, undergoing autobrecciation due to a still significant decrease in temperature and confining pressure. (**c**) As carbonated fluids keep migrating downslope, the autobrecciated terminations of these dykes are truncated and incorporated in the peperite. (**d**) The last dykes to be emplaced, after lateral migration of carbonated fluids had subsided, are not truncated. Carbonated fluids issued from the sides of several dykes keep mobilizing sands subsequent to dyke emplacement and to the lateral migration of peperite material.

7.2. Hydrothermal alteration

The abundance of K-feldspars in the least-altered basalt samples is surprising, considering that the trace element contents of these rocks suggest that they were derived from a sub-alkaline melt (Figure 3). However, the association of K-feldspars with relatively fresh rocks (Tables 1 and 2) does not suggest that they are the products of

hydrothermal alteration. These sub-alkaline melts were apparently enriched in alkalis prior to dyke emplacement (research in progress).

The increasing degree of mafic dyke alteration up towards the unconformity (Figure 5e) may be directly related to increasing porosity and associated water content in the host rocks, due to subsurface weathering. As a result, thorough albitization of the mafic rocks is only observed near or above the unconformity (Figure 5a).

Although cases of albitization by meteoric water have been described (Slaby *et al.* 1993; Hezarkhani and Williams-Jones 1998), the presence of saline water would best explain the observed replacement of Ca by Na in the feldspars. Schwartz and Surjono (1990) have reported fluid inclusions of high salinity in albitized granite, and Li Tongjin *et al.* (1985) have demonstrated experimentally that the mobility of K (or Na), Fe, Ca and Si (in decreasing order) is increased when gaseous thermal fluids are enriched in NaCl. The hyper-arid environment in which the Saint-Jules Formation was deposited (Jutras and Prichonnet 2002, 2004) is compatible with the inferred presence of saline groundwaters during magmatic emplacement.

The sudden disappearance of chlorite in mafic rocks located less than 7 m below the unconformity (Figure 5c) may indicate the approximate position of the palaeo-redox line in the aquifer during dyke emplacement. In the oxidizing conditions that prevailed above this line, chloritization gave way to thorough oxidation of the iron and titanium contents in the mafic rocks (Figure 5b, c).

The observed decrease in the ratios of $CaO/(Na_2O + K_2O)$ (Figure 5e) may be related to leaching by heated groundwater. The observation that mafic rocks are depleted in Ca near the unconformity suggests that the formation of ankerite at that level was probably related to a lack of available Ca (relative to CO_2) in these hot water brines.

7.3. Interpretation of stable isotope ratios

The carbon content in the ankerite veins below the unconformity (samples C1 and C2 on Figure 10) is too light to have been leached out of the marine Silurian host rocks, as marine calcite typically has a $\delta^{13}C$ VPDB value between -1 and 2 (Rollinson 1993). Hence, it probably reflects the carbon content of the local aquifer at the time of magmatic emplacement, which may have achieved light $\delta^{13}C$ values due to the presence of continental organic matter, especially below the redox line (Richardson and McSween 1989). However, the $\delta^{13}C$ values of samples C3–6 (Figure 10) are clearly different from those of samples C1–2, and the carbonate matrix of the peperite was therefore not exclusively derived from fluids issued from below the unconformity. The $\delta^{13}C$ values of samples C3–6 are heavier than the range of magmatic waters and correspond most closely to those of marine carbonates (Brownlow 1996).

As noted earlier, the protolith for the peperite is a petromict conglomerate mainly composed of calcareous marine sedimentary rock clasts according to field observations away from the dyke swarm. According to stable isotopes and field data, the most likely origin of the carbonate matrix in the peperite is therefore these clasts. A combination of the carbonate and siliciclastic–oxide matrices corresponds quite closely to the composition of these clasts. It is therefore concluded that the carbonate component of the calcareous gravels was dissociated from the siliciclastic and oxide fractions of these clasts during peperite formation above the dykes at localities 12 and 13 to form fluidal bands and globules of two distinct compositions. The physics of this fluidization will be discussed in a subsequent section.

The calcrete samples (samples C7a, C8 and C9 on Figure 10) should reflect the carbon content of groundwater above the water table at the time of calcrete formation, which records a period of increased aridity and low vegetation cover. In support of the latter conclusion, the calcrete hardpans are not disturbed by root traces. The calcretes probably developed within an arid and oxidizing environment that was poor in continental organic matter, which explains why their carbon content is heavier than in samples C1 and C2. The latter are interpreted to reflect the general carbon content of the aquifer below the water table, where organic matter is better preserved and where small-scale climatic fluctuations have less influence on water compositions. According to Dever *et al.* (1987), calcretes tend to show $\delta^{13}C$ and $\delta^{18}O$ values in the heavier part of the meteoric range due to their formation during periods that are characterized by high evaporation rates.

Due to the incorporation of calcrete material in the peperite matrix at localities 12 and 13 (Figure 6c), the carbon in the matrix may not be entirely of marine origin. The $\delta^{13}C$ values of samples C4 and C6 (Figure 10), which are in the lower range of marine carbonates and in the upper range of calcretes, possibly reflect a mixed derivation from calcrete and marine rock components.

The $\delta^{18}O$ values of carbonate material below and above the unconformity are very similar. The observation that sample C7 varies only in terms of its $\delta^{18}O$ values with different degrees of dissociation (samples C7a, b and c on Figure 10) suggests that the oxygen content of the carbonate matrix in the peperite was homogenized to values reflecting those of the ambient hydrothermal fluids. As carbon was much less abundant than oxygen in these hydrothermal fluids, the carbon content of the host rocks was not significantly homogenized. Hence, based on the observed variations in sample C7, the carbon content of the reconstituted carbonates in the peperite is thought to be representative of that of their source material, whereas its oxygen content is thought to reflect that of the hydrothermal fluids that probably circulated extensively in the system during dyke emplacement and cooling.

7.4. Interpretation of REE contents

The positive Eu anomaly in the sub-unconformity ankerite vein (sample C1 on Figure 11) may be due to the presence of *c*. 2% albite in that material (Table 1). Apart from this, the carbonate veins do not seem to have efficiently leached the host basalt, which is much richer in REEs (Figure 11).

The pronounced negative Ce anomaly of the carbonate vein (C1) is indicative of strongly oxidizing conditions, which favour the removal of Ce^{3+} from solution by converting it to its less soluble, oxidized form (Ce^{4+}) (Goldberg 1961). The much less pronounced negative Ce anomaly in the sandstone dyke sample (FS1 on Figure 11) may reflect input from ankerite veining below the unconformity, from which it apparently issued.

The marked difference in REE contents between the sub-unconformity ankerite vein (C1) and the carbonate matrix of the peperite (C3) is further evidence that they are not derived from the same source. Moreover, the similarity of REE contents in the carbonate matrix of the peperite (C3) and undisturbed clastic sediments of the Saint-Jules Formation (SS1) also concurs with carbon isotope analysis by implying that the former may be the product of disintegration of the latter.

7.5. Formation of ferrocarbonatites and associated 'fenitization'

Based on the following structural, textural and geochemical evidence, the carbonate matrix in the New-Carlisle peperite is interpreted to have crystallized from a melt, as opposed to being the result of hydrothermal processes.

- Above the dyke at locality 13, gravel clasts are supported by the micritic carbonate material, which forms the bulk (*c*. 60%) of the peperite volume at this locality (Figure 6a, c–e). We argue that this micrite-supported breccia could not have formed through the gradual precipitation of carbonate from saturated hot waters. A fluid with a higher viscosity than water was necessary to maintain gravel-size clasts in suspension prior to its cooling and rapid solidification.
- The dominantly massive micritic carbonate material shows flow textures in some areas (Figure 6a, c–e), but no lamination. We argue that to achieve a cement-supported framework, dissolution and precipitation from hydrothermal waters would likely have generated laminated carbonate because of the gradual nature of the process, as opposed to the massive and fluidal textures observed.
- Juvenile igneous clasts 'float' in the reconstituted carbonate and were therefore free to travel from the igneous body into the host sediment. This implies that the latter was fluidized and possibly molten. Hence, the carbonate matrix of the peperite could not be the result of gradual mineral replacement by infiltrating hydrothermal waters, as this process would not generate such effective mingling.
- The fluidized siliciclastic–oxide material and the carbonate were apparently immiscible (Figure 6c, d). As the fluidized siliciclastic–oxide material solidified first, it was incorporated as semi-brittle fragments of reconstituted sands and muds within the carbonate melt (Figure 6a, e). We argue that gradual mineral replacement by infiltrating

hydrothermal waters would have resulted in the dissemination of siliciclastic and oxide material within the carbonate, rather than their concentration into bands.

- The carbon isotope ratios of the carbonate matrix are not diluted enough compared to those of non-dissociated carbonate (Figure 6c and samples C7a–c on Figure 10) to support the hypothesis of mineral replacement by infiltrating hydrothermal waters that show significantly lighter isotopic ratios (samples C1–2 on Figure 10). For instance, sub-surface mineral replacement by meteoric groundwaters leaves carbon isotope ratios in the resulting calcrete that contrast sharply with those of their host rock remnants (Jutras *et al*. 1999).

Being dominantly composed of ankerite, the carbonate matrix of the peperite is here referred to as a ferrocarbonatite. Such melting of host sediment was reported in the case of several other peperites (Schminke 1967; Ito *et al.* 1984; Krynauw *et al.* 1988; Yamamoto *et al.* 1991; McPhie and Hunns 1995; WoldeGabriel *et al.* 1999; Martin and White 2002), and it could be argued that some of the textures and contact relationships described in Brooks *et al.* (1982) and Busby-Spera and White (1987) may constitute evidence of sediment melting, although this is not explicitly stated in their papers. Most of the igneous bodies involved in these previously reported cases of sediment melting in peperite are of comparable size or smaller than the 30-m-wide dyke at locality 13, where evidence of sediment melting is observed.

Wyllie and Tuttle (1960) determined that calcite can melt at temperatures as low as 740°C in the presence of abundant water, although the presence of CO_2 can greatly increase its melting temperature. Paterson (1958) observed that calcite melts between 900 and 1000°C in carbonated water, still well below the temperature of mafic melts. Hence, according to experimental data, carbonate melting at the contact of mafic magma can be expected if abundant water is present to favour heat transfer and reduce melting temperatures. Lentz (1999) concluded that carbonate melts can be derived from calcareous sedimentary rock skarns where magma intrudes a water-drenched environment, especially if the hydrothermal system is salty. At New-Carlisle, pervasive albitization suggests that salt concentrations were elevated during dyke emplacement, whereas low CO_2 concentrations are suggested by a high degree of oxygen contamination paired with a low degree of carbon contamination in the ferrocarbonatites (Figure 6c and samples C7a–c on Figure 10). Evidence for the presence of large amounts of water in the system during peperite formation will be discussed in a subsequent section.

As dyke emplacement at New-Carlisle resulted in carbonate melting under highly oxidizing conditions, certain parallels with carbonatite metasomatism (fenitization) can be drawn. The formation of hematite-rich albitites, for example, is typical of fenites (Coetzee 1963; Denaeyer 1966; Shimron 1975; Garson *et al.* 1984; Nambiar 1987; Ahijado and Hernandez 1992; Sood 1992; Rugless and Pirajno 1996). The observed high apatite and anatase contents in our igneous and peperitic rocks are also typical of carbonatite environments (Hogarth 1989).

Although certain parallels can be made with fenites, most carbonatites have substantially higher REE contents (Taylor *et al.* 1967; Martin *et al.* 1978; Cullers and Graf 1984; Wyllie 1989), especially ankeritic ones (Andersen 1984, 1986). However, such super-enrichment in REEs is characteristic of mantle-derived carbonate melts (Taylor *et al.* 1967; Loubet *et al.* 1972; Martin *et al.* 1978; Wyllie 1989) and is not to be expected for those rocks that are the products of calcareous rock melting in supracrustal successions.

7.6. Peperite formation

Prior to this study, the basal breccia at New-Carlisle was considered sedimentary (Bagdley 1956; Bourque and Lachambre 1980). As was noted by Squire and McPhie (2002), few peperites have been reported in coarse-grained sediments due to difficulties in differentiating them from undisturbed coarse sedimentary deposits. As in the case study by Squire and McPhie (2002), the peperites at New-Carlisle can be differentiated from sedimentary breccia by the observed mingling of sub-rounded sedimentary clasts and angular igneous clasts, with common jigsaw-fits (Figures 6a–c and 9b, g, h, j).

Very little 'globular' or 'fluidal' mingling of magma and sediment is observed in the peperites of New-Carlisle, which are essentially 'blocky', following the nomenclature proposed by Busby-Spera and White (1987). Blocky

textures are promoted by the high viscosity of a magma (Goto and McPhie 1996; Dadd and van Wagoner 2002; Squire and McPhie 2002). The New-Carlisle mafic melts must have been relatively viscous when they reached the Acadian unconformity, as suggested by their partly porphyritic texture (Figure 9f, h) and by the observation that some of the dykes terminate just below that level (Figure 9k). However, minor 'intermediate' peperite textures (ranging between blocky and globular in the nomenclature proposed by Hooten and Ort (2002)) are observed above the mafic dykes at localities 16 and 18, possibly due to a lower contrast in temperature between magma and host at the time of their formation. This hypothesis is supported by the observation that these are the only dykes to penetrate substantially above the unconformity.

Blocky textures are also promoted by the coarseness of the host sediments, which interferes with the formation of an insulating vapour film at the magma–sediment contact, thereby promoting heat diffusion (Busby-Spera and White 1987; Squire and McPhie 2002). Efficient heat diffusion must in turn have favoured sediment melting, which is interpreted to have occurred at localities 12 and 13, where all calcareous clasts are disintegrated. One notable exception is the presence of the partly preserved pedogenic calcrete hardpan and of a few incompletely digested clasts of this material (Figure 6c). The massive calcrete material was therefore seemingly harder to dissociate and melt than the calcareous gravels.

The dykes at localities 16 and 18 are examples of 'forceful magma intrusions' (*sensu* Skilling *et al.* 2002), in which the igneous bodies forcefully invaded the sedimentary body as a discrete mass (Figure 9a, e, f). The boulder-size basement rock slabs at the edge of the dyke at locality 18 (Figure 9f) were seemingly injected in the peperite as the dyke partly bulldozed its way through. Such injections of basement rock slabs (xenoliths) in peperite have not been previously reported in the literature.

There is no evidence for explosion in the process of peperite formation at New-Carlisle, such as massive, fines-depleted, pipe-like structures, or vesicular and 'ragged' juvenile clasts. Basalt fragmentation seemingly occurred by rapid quenching only, causing autobrecciation, decrepitation and spalling as the dykes reached the cold and wet Acadian unconformity, abruptly switching from a ductile to a brittle rheology (Goto and McPhie 1996). However, there is abundant evidence for fluidization of the host sediment, which has contributed greatly to the mingling of sedimentary and magmatic materials.

7.7. Migration of carbonate melt and carbonated water vapour

High feldspar, ankerite and rutile contents in the sandstone dykes (samples FS1, FS2 and FS4 in Table 1), which decline in concentration going up the profile (sample FS3 in Table 1) and which are not abundant in the host sediment (sample SS1 in Table 1), are clear indications of inputs from below the unconformity. The titanium oxides are mainly in the form of anatase within the mafic bodies (Table 1), but in the process of being incorporated within fluidized sediments, anatase was converted to the more stable mineral structure of rutile. Such vertical fluidization of sands (dykes of 'reconstituted sediments' *sensu* Krynauw *et al.* 1988; i.e. sediments that have undergone fluidization during peperite formation) has been observed in other peperite environments, where they are associated with fractures fed by the circulation of a water vapour film on the side of sills (Branney and Suthren 1988), but they are relatively uncommon in the literature. However, the New-Carlisle examples may provide the first observation of peperite formation atop dykes, which likely offer a better pathway than sills for a concentrated flow of buoyant water vapour to invade and fluidize the host sediments vertically.

Based on previous research by Paterson (1958), Wyllie and Tuttle (1960), and Lentz (1999), the profuse and focused intrusion of CO_2-poor waters derived from the sides of the dyke may have promoted carbonate melting in the sediments above the Acadian unconformity by reducing the melting temperature of calcite and by favouring heat transfer from the mafic bodies. The tight network of veins in the dykes, the homogenization of oxygen isotope ratios to that of hydrothermal vein values in the carbonate matrix of the peperite at locality 13, and the large volume of fluidized sediments are taken as evidence that water was indeed abundant and relatively free-flowing in the system.

Whereas the low density of vaporized water allowed it to travel vertically, it is unlikely that carbonate melts could travel far up into the aquifer due to their higher density than the interstitial water column above. This may explain the curving of carbonate melts to a horizontal flow (Figure 6f).

Due to its lack of buoyancy with respect to overlying groundwaters, the carbonate melt may have been forced to migrate 'downslope' along the unconformity surface, away from the basement uplift that was created by magmatic emplacement (the New-Carlisle inlier) (Figure 12a). It possibly evolved laterally from wet carbonate magma to Ca- and Fe-saturated water.

Mingling of low viscosity carbonate melt and/or saturated hydrothermal fluids with wet clastic sediments may be responsible for the oxidation of their iron and titanium contents. As a result, sand grains were thickly coated with hematite and rutile, a feature reported in the reconstituted sediments of other peperites (Brooks *et al.* 1982; Krynauw *et al.* 1988), and the crystallization of ankerite was gradually replaced by that of calcite. This gradual oxidation of the carbonated fluids is suggested by the observation that the carbonate cements of the sand dykes evolve upward from an ankeritic (sample FS2) to a calcitic (sample FS3) composition (Figure 9a and Table 1). Such oxidation of carbonate melt components by interactions with groundwater has also been observed during late stages of mantle-derived ferrocarbonatite emplacement, which leads to the formation of rodbergs ('red rocks') (Andersen 1984).

As was suggested earlier, the first dykes to be emplaced may have suddenly stopped rising at the unconformity due to an abrupt change in host material properties (Figure 12a), but dykes that were emplaced later, after the system had been already heated by previous emplacements, were able to extend slightly above the unconformity due to a reduced contrast in temperatures (Figure 12b). Less temperature contrast may also impede the formation of glass shards, which are mainly observed above the dyke at locality 13. The latter is therefore considered to be among the first dykes to be emplaced. This interpretation is supported by the observation that the dyke abruptly stops at the unconformity, even though it is considerably larger and was therefore capable of conveying more heat than other dykes during emplacement. This last consideration may in turn explain why substantial sediment melting is only observed in the vicinity of this dyke.

Although late dykes may have experienced a less drastic change in temperature at the unconformity during emplacement, they autobrecciated as they invaded the sedimentary basin due to a still significant decrease in temperature and confining pressure. Some of the dykes saw their strongly autobrecciated terminations truncated above the unconformity by the lateral movement of carbonate melts (and/or saturated hydrothermal fluids) and incorporated into the mobilized peperitic material (Figure 12c). This would explain the 'clouds' of juvenile clasts that are observed 'downslope' of each truncated dyke. It would also explain the abundant presence of composite clasts of mafic rock welded to gravels in peperite along the sloping unconformity surface (e.g. Figure 9h), as well as the lack of preserved structures of accommodation above the forceful intrusion of the dyke at locality 18 (Figure 9e). As for the dyke at locality 16, which is autobrecciated but not truncated above the unconformity, this intrusion may have been emplaced in late stages, when the lateral migration of carbonate melts (and/or saturated hydrothermal fluids) that were generated during the early emplacement of larger dykes had already ended in that area (Figure 12d).

The extent of lateral peperitic migration is marked by the abutting and folding of *in situ* sedimentary beds, *c.* 100 m east of the dyke at locality 20 (Figure 9p). When the fluid inputs became insufficient to mobilize gravel-size clasts, lateral migration became limited to sand-size material, which infiltrated between coarser peperitic material (Figure 9m), but could not penetrate the uplifted *in situ* beds shown in Figure 9p. Because these beds seemingly acted as a rigid block to fluid migration, and because they are rich in easily cemented calcareous clasts, it is likely that they were relatively well consolidated prior to peperite formation.

A certain degree of eodiagenetic consolidation of the host sediment prior to magmatic emplacement has also been inferred for peperites developed in chert (Brooks *et al.* 1982) and carbonate micrite (Busby-Spera and White 1987). High porosity and water content may therefore be more crucial to the formation of peperite than looseness of sediments, although the thorough compaction that occurs during mesodiagenesis appears to impede their formation. This last consideration is suggested by a lack of peperitic textures in the more indurated Silurian mudstones at New-Carlisle.

The vertically fluidized sands (sandstone dykes) truncate the laterally displaced peperite and sandstone sills (Figure 9n), and therefore outlasted the lateral, 'downslope' migration of fluids (Figure 12d). These highly buoyant late fluids are an indication that the remainder of the peperite mass had stabilized when the system was still quite hot.

In contrast to the sandstone dykes at localities 12 (Figure 6f), 14, 16 (Figure 9a), 17 (Figure 9c) and 20 (Figure 9n), which transgress downward into ankerite veins below the unconformity, the sandstone dyke near locality 1 extends down into the Silurian basement for at least 1 m. This relationship is reminiscent of similar sandstone dykes that are frequently found at the base of the Saint-Jules Formation, away from the New-Carlisle dyke swarm, where they passively infill fractures in the basement (Jutras and Prichonnet 2004). However, these basal sandstone dykes do not extend upward into the Saint-Jules Formation, in contrast to the sandstone dyke near locality 1. This suggests that a pre-existing clastic dyke at that locality provided a pathway for hydrothermal fluids associated with the New-Carlisle intrusions to extend upward into the Saint-Jules Formation strata. According to this interpretation, truncation of the sandstone dyke by the Viséan Bonaventure Formation provides evidence that the mafic intrusions are no younger than Viséan. A younger age for the Bonaventure Formation than for the New-Carlisle dykes is also supported by the presence of abundant mafic rock and ankerite clasts in the lowermost conglomerate beds of the Bonaventure Formation near the New-Carlisle inlier (Jutras and Prichonnet 2004).

8. SUMMARY AND CONCLUSIONS

Upper Palaeozoic mafic melts experienced drastic chemical and mechanical transformations when they reached the Acadian unconformity during dyke emplacement in the New-Carlisle area of eastern Quebec. They underwent chloritization below the palaeo-redox line, and thorough oxidation and albitization above this line.

The basal beds of the Saint-Jules Formation, at and near the contact with the dykes, show several of the characteristic features of peperite as summarized by Skilling *et al.* (2002). These include forceful magma intrusion (Figure 9a, e, f), jigsaw-fit autobrecciation of magma (Figures 6b, c and 9b), mingling of juvenile clasts and sediments (Figures 6a–c and 9h, j), sediment fluidization (Figures 6a, c–f and 9a, c, d, m, n, p), and sediment melting (Figure 6a, c–e).

One feature that was not previously reported is the forceful injection of basement slabs (xenoliths) into the peperite (Figure 9f), which may be related to the fact that, in contrast to most peperite cases documented to date, the New-Carlisle peperites are associated with dykes rather than with sills or invasive lava flows. It is mechanically easier for xenoliths to be transferred to the peperite by dyke intrusions. We also argue that more heat can be concentrated above a dyke than above a sill because the sides of a dyke provide efficient and focused pathways for heated waters to invade the sedimentary basin above the unconformity, all of which may have promoted melting of the carbonate components in the calcareous clastics of the Saint-Jules Formation, locally generating large volumes of carbonate melts. Circulation of these carbonate melts along the Acadian unconformity seems to have been gravity-controlled. It may be responsible for the observed truncation of some of the dykes by peperitic breccia (Figure 9c, e, n) and for the efficient mingling of juvenile igneous clasts with sediments over a large area.

ACKNOWLEDGEMENTS

We wish to thank J. McKay for stable isotope analyses, L. Harnois for INAA analyses, and J. Bourne, D. Lentz, S. McCutcheon, G. Pe-Piper, D. J. W. Piper and R. Stevenson for fruitful discussions in early stages of this project, which was supported by a Discovery grant of the Natural Sciences and Engineering Research Council (NSERC) of Canada to P. Jutras. We also wish to thank J. D. L. White, C. Shaw and an anonymous reviewer for their constructive reviews.

REFERENCES

Ahijado A, Hernandez PA. 1992. El Complejo ultramagnifico-carbonatico del macizo de Amanay, Fuerteventura, Islas Canarias. *Actas del Congresso Latinoamericano de Geologia* **8**: 315–318.

Andersen T. 1984. Secondary processes in carbonatites: petrology of rodbergs (hematite-calcite-dolomite carbonatite) in the Fen central complex, Telemark (South Norway). *Lithos* **17**: 227–245.

Andersen T. 1986. Compositional variation of some rare earth minerals from the Fen complex (Telemark, SE Norway): implications for the mobility of rare earths in a carbonatite system. *Mineralogical Magazine* **50**: 503–509.

Bagdley PC. 1956. *New Carlisle Map-Area; electoral district of Bonaventure:* Quebec Department of Mines, RG-70.

Boulter CA. 1993. High-level peperitic sills at Rio Tinto, Spain; implications for stratigraphy and mineralization. *Transactions of the Institution of Mining and Metallurgy (Section B: Applied Earth Sciences)* **102**: 30–38.

Bourque PA, Lachambre G. 1980. *Stratigraphie du Silurien et du Dévonien basal du sud de la Gaspésie*. Ministère de l'Énergie et des Ressources du Québec, ES-30.

Branney MJ, Suthren RJ. 1988. High-level peperitic sills in the English Lake District; distinction from block lavas, and implications for Borrowdale Volcanic Group stratigraphy. *Geological Journal* **23**: 171–187.

Brownlow AH. 1996. *Geochemistry* (2nd edn). Prentice-Hall: Upper Saddle River.

Brooks ER. 1995. Palaeozoic fluidization, folding, and peperite formation, northern Sierra Nevada, California. *Canadian Journal of Earth Sciences* **32**: 314–324.

Brooks ER, Wood MM, Garbutt PL. 1982. Origin and metamorphism of peperite and associated rocks in the Devonian Elwell Formation, northern Sierra Nevada, California. *Geological Society of America Bulletin* **93**: 1208–1231.

Busby-Spera CJ, White JDL. 1987. Variation in peperite textures associated with differing host-sediment properties. *Bulletin of Volcanology* **49**: 765–776.

Coetzee GL. 1963. Carbonatites of the Karema depression, western Tanganyika. *Transactions of the Geological Society of South Africa* **66**: 283–340.

Coira B, Perez B. 2002. Peperitic textures of Ordovician dacitic synsedimentary intrusions in Argentina's Puna Highland; clues to emplacement conditions. *Journal of Volcanology and Geothermal Research* **114**: 165–180.

Cullers RL, Graf JL. 1984. Rare earth elements in igneous rocks of the continental crust: predominently basic and ultrabasic rocks. In *Rare Earth Element Geochemistry*, Henderson P (ed.). Elsevier: Amsterdam; 237–274.

Dadd KA, van Wagoner NA. 2002. Magma composition and viscosity as controls on peperite texture; an example from Passamaquoddy Bay, southeastern Canada. *Journal of Volcanology and Geothermal Research* **114**: 63–80.

Denaeyer ME. 1966. Sur la présence d'une carbonatite ankéritique (rauhaugite) en bordure du complexe alcalin de Kirumba (Kivu). *Comptes-rendus de l'Académie des Sciences, Série D, Sciences Naturelles* **263**: 9–12.

Dever L, Fontes JC, Riché G. 1987. Isotopic approach to calcite dissolution and precipitation in soils under semi-arid conditions. *Chemical Geology* **66**: 307–314.

Doyle MG. 2000. Clast shape and textural associations in peperite as a guide to hydromagmatic interactions; Upper Permian basaltic and basaltic andesite examples from Kiama, Australia. *Australian Journal of Earth Sciences* **47**: 167–177.

Garson MS, Coats NM, Rock NMS, Deans T. 1984. Fenites, breccia dykes, albitites, and carbonatitic veins near the Great Glen Fault, Inverness, Scotland. *Journal of the Geological Society of London* **141**: 711–727.

Goldberg Ed. 1961. Chemistry in the Oceans. In Oceanography, Sears M (ed.). *American Association for the Advancement of Science* **67**: 583–597.

Goto Y, McPhie J. 1996. A Miocene basanite peperitic dyke at Stanley, northwestern Tasmania. *Australian Journal of Volcanology and Geothermal Research* **74**: 111–120.

Hanson RE, Schweickert RA. 1982. Chilling and brecciation of a Devonian rhyolite sill intruded into wet sediments, northern Sierra Nevada, California. *Journal of Geology* **90**: 717–724.

Hanson RE, Wilson TJ. 1993. Large-scale rhyolite peperites (Jurassic, southern Chile). *Journal of Volcanology and Geothermal Research* **54**: 247–264.

Hezarkhani A, Williams-Jones AE. 1998. Controls of alteration and mineralization in the Sungun porphyry copper deposit, Iran: evidence from fluid inclusions and stable isotopes. *Economic Geology* **93**: 651–670.

Hogarth DD. 1989. Pyrochlore, apatite and amphibole; distinctive minerals in carbonatite. In *Carbonatites; Genesis and Evolution*, Bell K (ed.). Unwin Hyman: London; 105–148.

Hooten JA, Ort MH. 2002. Peperite as a record of early-stage phreatomagmatic fragmentation processes; an example from the Hopi Buttes volcanic field, Navajo Nation, Arizona, USA. *Journal of Volcanology and Geothermal Research* **114**: 95–106.

Ito T, Matsumoto R, Kano K, Sakuyama M. 1984. Welding of acidic tuff and altered rhyolite fragments caused by the intrusion of magma: examples in the Neogene Shirahama Group, south Izu, Japan. *Journal of Volcanology and Geothermal Research* **37**: 59–75.

Jutras P, Prichonnet G. 2002. Stratigraphy, depositional setting and diagenetic history of the Saint-Jules Formation (Upper Devonian or Mississippian), a newly identified post-Acadian red clastic unit in the southern Gaspé Peninsula, Québec. *Canadian Journal of Earth Sciences* **39**: 1541–1551.

Jutras P, Prichonnet G. 2004. Significance of paleosurfaces in interpreting the paleogeographic and stratigraphic evolution of the upper Palaeozoic Paspébiac Graben, a recently identified basin in the southern Gaspé Peninsula of Quebec, Canada. *Geological Society of America Bulletin* **116**: 1074–1086.

Jutras P, Prichonnet G, von Bitter P. 1999. The La Coulée Formation, a new post-Acadian continental clastic unit bearing groundwater calcretes, Gaspé Peninsula, Québec. *Atlantic Geology* **35**: 139–156.

Jutras P, Prichonnet G, Utting J. 2001. Newly identified Carboniferous units (The Pointe Sawyer and Chemin-des-Pêcheurs formations) in the Gaspé Peninsula, Québec; Implications regarding the evolution of the northwestern sector of the Maritimes Basin. *Canadian Journal of Earth Sciences* **38**: 1–19.

Kano KI. 1989. Interactions between andesitic magma and poorly consolidated sediments; examples in the Neogene Shirahama Group, South Izu, Japan. *Journal of Volcanology and Geothermal Research* **37**: 59–75.

Kokelaar BP. 1982. Fluidization of wet sediments during the emplacement and cooling of various igneous bodies. *Journal of the Geological Society of London* **139**: 21–33.

Kokelaar BP. 1986. Magma-water interactions in subaqueous and emergent basaltic volcanism. *Bulletin of Volcanology* **48**: 275–289.

Krynauw JR, Hunter DR, Wilson AH. 1988. Emplacement of sills into wet sediments at Grunehogna, western Dronning Maud Land, Antarctica. *Journal of the Geological Society of London* **145**: 1019–1032.
Leat PT, Thompson RN. 1988. Miocene hydrovolcanism in NW Colorado, USA, fuelled by explosive mixing of basic magma and wet unconsolidated sediment. *Bulletin of Volcanology* **50**: 229–243.
Lentz DR. 1999. Carbonatite genesis: a reexamination of the role of intrusion-related pneumatolytic skarn processes in limestone melting. *Geology* **27**: 335–338.
Loubet M, Bernat M, Javoy M, Allègre CJ. 1972. Rare earth contents in carbonatites. *Earth and Planetary Science Letters* **14**: 226–232.
Li Tongjin, Lu Jialan, Zhao Bin, Yi Dongshan 1985. Experimental studies of leaching and albitization in intermediate-basic rocks. *Chemical Geology* **49**: 115–125.
Martin RF, Whitley JE, Woolley AR. 1978. An investigation of rare earth mobility: fenitized quartzites, Borralan Complex, N.W. Scotland. *Contributions to Mineralogy and Petrology* **66**: 69–73.
Martin U, White JDL. 2002. Melting and mingling of phonolitic pumice deposits with intruding dykes: an example from the Otago Peninsula, New Zealand. *Journal of Volcanology and Geothermal Research* **114**: 129–146.
McClintock MK, White JDL. 2002. Granulation of weak rock as a precursor to peperite formation; coal peperite, Coombs Hills, Antarctica. *Journal of Volcanology and Geothermal Research* **114**: 205–217.
McPhie J, Hunns SR. 1995. Secondary welding of marine, pumice-lithic breccia at Mount Chalmers, Queensland, Australia. *Bulletin of Volcanology* **57**: 170–178.
Nambiar AR. 1987. Alkaline magmatism in parts of West Khasi Hills and East Garo Hills districts, Meghalaya. *Recordings of the Geological Survey of India* **115**: 25–44.
Okulitch AV. 1999. Geological time chart 1999. In *The National Earth Science Series Geological Atlas*, Okulitch AV (ed.). Geological Survey of Canada Open-File 3040, Revision from GEOLOG, 29, part I.
Paterson MS. 1958. The melting of calcite in the presence of water and carbon dioxide. *The American Mineralogist* **43**: 603–606.
Richardson SM, McSween HY Jr. 1989. *Geochemistry; Pathways and Processes*. Prentice-Hall: Englewood Cliffs.
Rollinson HR. 1993. *Using Geochemical Data; Evaluation, Presentation, Interpretation*. Longman Scientific & Technical: Harlow.
Rugless CS, Pirajno F. 1996. Geological [sic] and geochemistry of the Copperhead albitite-'carbonatite' complex, East Kimberley, Western Australia. *Australian Journal of Earth Sciences* **43**: 311–322.
Schminke HU. 1967. Fused tuff and peperites in south-central Washington. *Geological Society of America Bulletin* **78**: 319–330.
Schwartz MO, Surjono. 1990. Greisenitization and albitization at the Tikus tin-tungsten deposit, Belitung, Indonesia. *Economic Geology* **85**: 691–713.
Shimron AE. 1975. Petrogenesis of the Tarr albitite-carbonatite complex, Sinai Peninsula. *Mineralogical Magazine and Journal of the Mineralogical Society* **40**: 13–24.
Skilling IP, White JDL, McPhie J. 2002. Peperite; a review of magma-sediment mingling. *Journal of Volcanology and Geothermal Research* **114**: 1–17.
Slaby E, Kozlowski A, Lenach G, Mihm A. 1993. Origin of albite-adularia paragenesis: an example of alkali metasomatism through magmatic-meteoric fluid mixing. *Mineralogia Polonica* **24**: 3–19.
Sood NK. 1992. Petrography and metallogeny of the albitite-ultramafic-carbonatite province of northeastern Rajasthan. *Recordings of the Geological Survey of India* **124**: 92.
Squire RJ, McPhie J. 2002. Characteristics and origin of peperite involving coarse-grained host sediment. *Journal of Volcanology and Geothermal Research* **114**: 45–61.
Taylor HP Jr, Frechen J, Degens ET. 1967. Oxygen and carbon isotope studies of carbonatites from the Laacher See district, West Germany, and the Alnö district, Sweden. *Geochimica et Cosmochimica Acta* **31**: 407–430.
Winchester JA, Floyd PA. 1977. Geochemical discrimination of different magma series and their differentiation products using immobile elements. *Chemical Geology* **20**: 325–343.
WoldeGabriel G, Keating GN, Valentine G. 1999. Effects of shallow basaltic intrusion into porphyritic deposits, Grants Ridge, New Mexico, USA. *Journal of Volcanology and Geothermal Research* **92**: 389–411.
Wyllie PJ. 1989. Origin of carbonatites: evidence from phase equilibrium studies. In *Carbonatites; genesis and evolution*, Bell K (ed.). Unwin Hyman: London; 500–545.
Wyllie PJ, Tuttle OF. 1960. The system CaO-CO (sub 2) -H (sub 2) O and the origin of carbonatites. *Journal of Petrology* **1**: 1–46.
Yamamoto T, Soya T, Suto S, Uto K, Takada A, Sakguchi K, Ono K. 1991. The 1989 submarine eruption of eastern Izu Peninsula, Japan: ejecta and eruption mechanisms. *Bulletin of Volcanology* **53**: 301–308.

Scientific editing by Ron Pickerill

